Master-Thesis an der Hochschule Luzern - Technik & Architektur

Titel	**Open-source application for design, simulation and analysis of multi-component gas adsorption processes in fixed bed columns**
Diplomandin/Diplomand	**Blättler, Roman**
Master-Studiengang	**Master in Engineering**
Semester	**HS21**
Dozentin/Dozent	**Kleingries, Mirko**
Expertin/Experte	**Guidati, Gianfranco**

Abstract Deutsch
Adsorptionsprozesse gehören zu den wichtigsten verfahrenstechnischen Methoden für die großindustrielle Gastrennung und -reinigung. Jüngste Entwicklungen in der Trenntechnik haben neue Verfahrenskonzepte und neue Adsorbentien hervorgebracht, die attraktive Eigenschaften hinsichtlich Energiebedarf, Durchsatz, Regeneration des Adsorbens und Reinheit des Produkts bieten. Für optimal ausgelegte Adsorptionsprozesse werden zunehmend mathematisch-physikalische Modelle und Simulationssoftware eingesetzt. Im Rahmen dieser Masterarbeit wurde eine auf Open Source basierte Anwendung für die Auslegung, Simulation und Analyse von Mehrkomponenten-Gasadsorptionsprozessen in Festbettkolonnen entwickelt. Das speziell entwickelte Adsorptionsmodell wurde anhand eines gemessenen Referenzfalles für die Abtrennung von CO_2 und N_2 aus He an Aktivkohle erfolgreich validiert. Das Modell kombiniert Massen-, Energie- und Impulsbilanzen mit einem linear-driving-force Ansatz für den Stoff- und Wärmetransport. Die Gleichgewichtsbeladungen wurden mit der erweiterten Langmuir-Gleichung modelliert und die beladungsabhängigen Adsorptionsenthalpien mittels der isosteren Methode berechnet. Basierend auf einem erstellten Konzept wurde die Anwendersoftware mit grafischen Benutzeroberflächen in Python implementiert. Der derzeitige Funktionsumfang der Software erlaubt im Wesentlichen die Eingabe aller definierten Parameter und Messdaten, die Modellierung von Adsorptionsgleichgewichten, die Simulationsdurchführung des entworfenen Adsorptionsprozesses sowie die grafische Auswertung der Simulationsergebnisse anhand von Massentransferzonen und Durchbruchskurven.

Abstract Englisch
Adsorption processes are among the most important process engineering methods for large scale gas separation and purification tasks in industry. Recent developments in separation technology have included new process designs and new adsorbents which offer attractive characteristics regarding energy demand, throughput, regeneration of the adsorbent and purity of the product. For optimum designed adsorption processes, mathematical-physical models and simulation software are increasingly used. Within this master thesis, an open-source based application was developed for the design, simulation and analysis of multi-component gas adsorption processes in fixed bed columns. The specially developed adsorption model was successfully validated using a measured reference case for the separation of CO_2 and N_2 from He on activated carbon. The model combines mass, energy and momentum balances with a linear driving force approach for mass and heat transport. The equilibrium loadings are modelled with the extended Langmuir equation and the loading dependent enthalpies of adsorption are calculated via the isosteric method. Based on a created concept, the user software with graphical user interfaces was implemented in Python. The current functional framework of the software basically allows the input of all defined parameters and measurement data, the modelling of adsorption equilibria, the simulation execution of designed adsorption process as well as the graphical evaluation of simulation results based on mass transfer zones and breakthrough curves.

Ort, Datum Horw, 21. Januar 2022

Lucerne University of
Applied Sciences and Arts

HOCHSCHULE
LUZERN

Technik & Architektur

MSE | MASTER OF SCIENCE
IN ENGINEERING

Master Thesis

Open-source application for design, simulation and analysis of multi-component gas adsorption processes in fixed bed columns

Roman Blättler

Advisor:	Prof. Dr. Mirko Kleingries
Expert:	Dr. Gianfranco Guidati
Scientific Partner:	CC Thermal Energy Systems and Process Engineering Research Group SORPTION
Date of Submission:	Horw, 21st January 2022

Contents

List of Symbols and Abbreviations

Latin Symbols

A	Surface area, cross-section	m^2
A_{ssa}	Volume specific surface area	m^2/m^3
c_p	Specific heat capacity	$J/(kgK)$
d	Diameter	m
D	Diffusion coefficient	m^2/s
E	Energy	J
h	Specific enthalpy	$J/kg, J/mol$
H	Enthalpy	J
$\dot{H}$	Enthalpy flow	W
Δh_{ads}	isosteric enthalpy of adsorption	$J/kg, J/mol$
K	Isotherm parameter	$-$
k_h	Overall heat transport coefficient	$W/(m^2K)$
k_m	Overall mass transport coefficient	m/s
L	Length	m
m	Mass	kg
$\dot{m}$	Mass flow	kg/s
M	Molar mass	$g/mol, kg/kmol$
n	amount of elements	$-$
p	pressure	Pa, bar
$\dot{Q}$	Heat flow	W
R	Gas constant	$J/(molK)$
T	Temperature	K
t	Time	s
v	Velocity	m/s
V	Volume	m^3
$\dot{V}$	Volume flow	m^3/s
X	Loading	$kg/kg, mmol/g$
z	Position of volume element	m
dz	element thickness	m

Greek Symbols

α	Convective heat transfer coefficient	m/s
β	Convective mass transfer coefficient	$W/(m^2K)$
ε_{bed}	bed porosity	$-$
ε_p	particle porosity	$-$
μ	Dynamic viscosity	$Pa\,s$
λ	Thermal conductivity	$W/(mK)$
λ_{free}	Free path length	m
Ω	Collision integral	$-$
ρ	Density	kg/m^3
ρ_g, ρ_n	Gross/net density of particle	kg/m^3
σ	Collision diameter	Å

Indices

a	Adsorptive
ads	Adsorption
ax	Axial
b	Bulk / carrier gas
c	Convection
d	Diffusion
eq	Equilibrium
g	Gas phase
k	Knudsen
l	Viscous (laminar)
p	particle
s	Solid phase, adsorbent
st	Storage
w	Wall

Abbreviations

BTC	Breakthrough curve
LDF	Linear driving force
MTZ	Mass transfer zone

Dimensionless Numbers

Nu	Nusselt number
Pr	Prandl number
Re	Reynolds number
Sh	Sherwood number
Sc	Schmidt number

Open-source application for design, simulation and analysis of multi-component gas adsorption processes in fixed bed columns

Roman Blättler

Lucerne University of Applied Sciences & Arts
School of Engineering and Architecture
Competence Center Thermal Energy Systems and Process Engineering
Research Group SORPTION
Technikumstrasse 21, CH-6048 Horw, Switzerland
roman.blaettler@hslu.ch

Abstract

Adsorption processes are among the most important process engineering methods for large scale gas separation and purification tasks in industry. Recent developments in separation technology have included new process designs and new adsorbents which offer attractive characteristics regarding energy demand, throughput, regeneration of the adsorbent and purity of the product. For optimum designed adsorption processes, mathematical-physical models and simulation software are increasingly used. Within this master thesis, an open-source based application was developed for the design, simulation and analysis of multi-component gas adsorption processes in fixed bed columns. The specially developed adsorption model was successfully validated using a measured reference case for the separation of CO_2 and N_2 from He on activated carbon. The model combines mass, energy and momentum balances with a linear driving force approach for mass and heat transport. The equilibrium loadings are modelled with the extended Langmuir equation and the loading dependent enthalpies of adsorption are calculated via the isosteric method. Based on a created concept, the user software with graphical user interfaces was implemented in Python. The current functional framework of the software basically allows the input of all defined parameters and measurement data, the modelling of adsorption equilibria, the simulation execution of designed adsorption process as well as the graphical evaluation of simulation results based on mass transfer zones and breakthrough curves.

1 Introduction

In the following, the background of this project is explained and the objectives and the methodology are set out.

1.1 Background

Gas separation and purification on large scale is an important task of many industrial processes. Process technologies developed for such purpose are cryogenic distillation, membrane separation, absorption and adsorption [1, 2]. This work focuses on gas phase adsorption processes in fixed bed columns. Common applications are gas separations such as volatile organic compounds from polluted air [3], or methane and carbon dioxide from combustion processes, biogas or atmosphere [4–6], among others also in combination with power-to-X systems or carbon capture and storage (CCS) [7]. In particular, the removal of carbon dioxide is an important process in the industry for reducing their environmental footprint.

Current developments in separation technology by adsorption have included new process designs and new structured adsorbents which offer attractive characteristics. These improvements feature lower energy demand, higher throughput, more selective separations, superior regeneration and enhanced purity of the product [8]. It is evident, that the advancement of adsorption processes will improve existing and evoke new applications in the production and energy sectors [9–12] and will make a significant contribution to compliance with future emission regulations and environmental protection directives [13–15].

Considering the design of adsorption processes, the knowledge of both thermodynamic and kinetic parameters is essential, besides the adsorber geometry and material structure. Gas adsorption is a non-isothermal process and highly complex, not least because of simultaneous mass and heat transport mechanisms at and within the adsorbent material and especially when multi-component adsorption takes place [16]. This induces a characteristically complex dynamic behaviour of the adsorber. The key questions in adsorber designs are: "When does the adsorber need to be regenerated?" or "How can the process be further optimised?"

However, the precise combination of these design parameters for optimum adsorption performance is often unknown in industry and belongs to current research [8]. Mathematical models are increasingly required to predict the performance of adsorptive separation systems and to optimise the design and opera-

tion of those plants [17]. Commercial process simulation software supporting this purpose are in use, e. g. *ADSIM®*, *AdDesignS®*, *gProms®*or *ProSim DAC®*. In industrial development of adsorption processes, nevertheless, shortcut and scale-/numbering-up methods, which are often based on already specified process concepts, are more commonly preferred over simulations of new process designs.

This master thesis builds on previous student work [18, 19] and is thematically correlated with all projects of the research group SORPTION, in which fixed bed adsorbers for material separation are investigated. Examples are R&D projects like SYSKON [20] and EESP [21, 22] or service contracts with companies such as Climeworks AG or Givaudan AG.

1.2 Objectives

The main objective of this master thesis is a software for design, simulation and analysis of gas adsorption processes in fixed bed columns.

A kinetic 1D model is to be developed that represents multi-component gas adsorption processes. Based on the simple adsorber model elaborated in the previous work, an advanced mathematical-physical calculation, visualization and evaluation are to be carried out. Starting from user defined design parameters for geometry, material and process condition, the programme is intended to simulate and visualise the characteristic process variables in a temporally and spatially resolved manner. Effects of parameter variations should be shown in diagrams that illustrate the sorption behaviour. In concrete terms, the mass transfer zone, heat waves and the breakthrough curves are to be plotted.

The programming should be open-source based and the tool capabilities are placed in between commercial simulation software and common short cut methods, i. e. it is a trade-off among fast and precise execution of design, simulation and analysis of the process. The software shall also support the user in preparing important thermodynamic and material data, exporting the simulation data and evaluating the results graphically. These goals shall be achieved with a comprehensible and straightforward application with an appealing graphical user interface (GUI). Suitable software functions should be equipped with proper GUI widgets regarding inputs, outputs and user interactions.

1.3 Methodology

To achieve the above mentioned objectives, the following steps were pursued.

1. Requirements specification

In cooperation with stakeholders, a tabular specification is created that includes all extended application functionalities. These may include multi-component adsorption, momentum transport in the adsorber, efficiency evaluations of individual adsorption/desorption processes as well as entire cycles and possibly an embedding of the functionalities in the guidelines of the EESP project. The specification sheet is divided into "Modelling & Simulation" and "Software & Graphical User Interface".

2. Familiarisation and literature research

In order to model the process, the technical and thermodynamic fundamentals must be researched and processed. Focus is laid on conservation equations, thermodynamic equilibria of multi-components as well as heat and mass transport. For the software realisation, the knowledge about programming and numerical methods must be ensured. In addition, the basics and the state of the art of graphical user interfaces must be acquired.

3. Modelling of adsorption processes

The correlations for the model functions, as defined in the specifications, are developed and documented. The simulation model reflects the current state of modelling and uses existing approaches. The conservation equation based PDEs need to be derived and discretised for implementation. The physical-technical correlations required to map equilibria and kinetics are composed and described in form of mathematical equations.

4. Conceptual design of GUI

Based on the findings of work package 2, concepts for the implementation of the interface will be developed and evaluated. The best evaluated concept will be implemented in work package 5.

5. Software realisation in Python

The adsorption process model, the software functionalities and the graphical user interface are realised in Python programming language. The simulation results obtained are also validated with measurement data from the literature to confirm the model accuracy.

2 Adsorption fundamentals

The driving force in adsorption processes, as in all thermal separation processes, is an externally imposed imbalance. The system tries to compensate this during the process by reaching a new state of thermodynamic equilibrium. The rate at which this process will occur is described by kinetics. Regarding the non-isothermal behaviour of gas phase adsorption, equilibrium and kinetics have significant influence on the dynamics and further play key role in the design of adsorption systems [16, 23]. But also the choice of suitable adsorbent materials and regeneration methods are decisive. These aspects are presented in this chapter.

2.1 Basic concept of adsorption

In general, adsorption refers to the accumulation of substances (adsorptives) from a liquid or gas on the surface of solids (adsorbents), resulting in the formation of a two-component system (adsorbate) while releasing enthalpy of adsorption Δh_{ads}. These surfaces are in particular the inner surfaces of porous solids. The reversal process is called desorption or regeneration of the adsorbent. In this work, only gas phase adsorption is considered.

$$\text{adsorptive} + \text{adsorbent} \longleftrightarrow \text{adsorbate} + \Delta h_{ads}$$

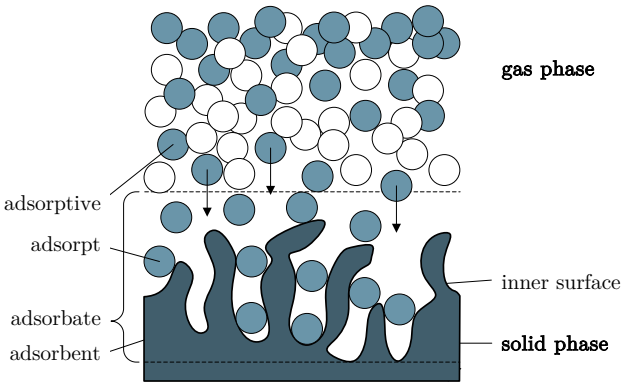

Figure 2.1: Basic concept of adsorption

Further technical terms used in this work are explained in more detail in appendix A.1.

2.2 Conservation equations

To describe transport of mass, energy or momentum in technical systems precisely, conservation equations are used. Conservation equations are applied on the balance areas. Consider a control volume, as shown in figure 2.2, with sides of $\delta x, \delta y, \delta z$ at position (x, y, z) as the smallest possible element within the system. All properties are functions of space and time. So $\rho(x, y, z, t)$, $p(x, y, z, t)$, $T(x, y, z, t)$ and $\mathbf{u}(x, y, z, t)$ for density, pressure, temperature and velocity vector. The general form of a differential balance equation is defined as

$$\underbrace{\frac{d\Phi}{dt}}_{storage} = \underbrace{-\nabla(\Phi\mathbf{u})}_{advection} + \underbrace{\nabla(\Gamma\nabla\Phi)}_{diffusion} + \underbrace{S_\Phi}_{source} \tag{2.1}$$

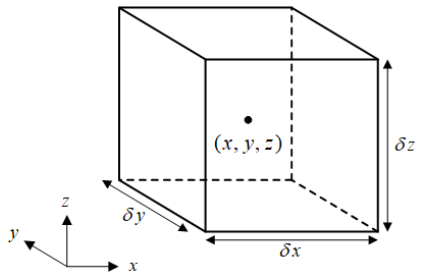

Figure 2.2: Control volume for balancing equations

with Φ as a representative balance quantity for mass, species, energy and momentum, the diffusion coefficient Γ and the source term S_Φ. Depending on the balanced quantity, Φ, Γ and S_Φ can be expressed according to table 2.1.

Table 2.1: Balance quantities

quantity	Φ	Γ	S_Φ
mass	$\rho[\frac{kg}{m^3}]$	-	-
species	$c_i[\frac{mol}{m^3}]$	$D_i[\frac{m^2}{s}]$	$S_{ci}[\frac{mol}{m^3 s}]$
energy	$h[\frac{J}{m^3}]$	$a[\frac{m^2}{s}]$	$S_h[\frac{W}{m^3}]$
momentum	$\rho u[\frac{Ns}{m^3}]$	$\nu[\frac{m^2}{s}]$	$S_{\rho u}[\frac{N}{m^3}]$

The momentum balance in table 2.1 only applies for one direction within the three-dimensional space. Since $\mathbf{u}(x, y, z) = (u(x, y, z), v(x, y, z), w(x, y, z))$, the momentum balances as to be considered in all direction in general.

2.3 Thermodynamic equilibrium

A system is in thermodynamic equilibrium when a stationary state prevails, i. e. all flows of matter and energy within the system disappear. The equilibrium state of adsorption, more specifically the adsorption capacity, has the following functional relationship.

$$f(p_a, X, T) = 0 \tag{2.2}$$

with the partial pressure p_a of the adsorptive, the loading X of the adsorbent with adsorbt and the temperature T of the adsorbent. For the case of multicomponent adsorption, p_a and X summarise all partial pressures $p_{a,i}$ resp. all partial loadings X_i.

Adsorption equilibrium can be represented in three functional ways [16, 23], as figure 2.3 shows:

$$\text{Isotherms:} \quad X = f(p_a)_T,\ T = const. \tag{2.3}$$

$$\text{Isosteres:} \quad p_a = f(T)_X,\ X = const. \tag{2.4}$$

$$\text{Isobars:} \quad X = f(T)_p,\ p = const. \tag{2.5}$$

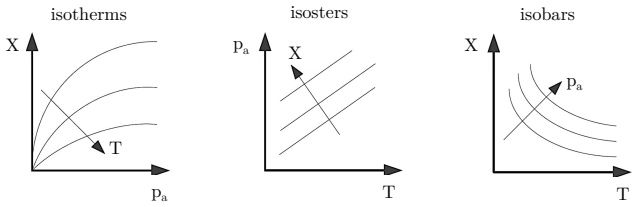

Figure 2.3: Representation of adsorption equlibrium [16]

2.3.1 Single-component isotherms

The single-component case is the simplest case of adsorption. In industry, this occurs only rarely; multi-component processes are the usual case. Although, it is often assumed that certain components behave inertly or that adsorption can be reduced to a leading component that consolidates the similar properties of the other adsorptives.

Isotherms are commonly used to describe adsorption equilibria. They are classified into six groups according to their shape, as depicted in figure 2.4:

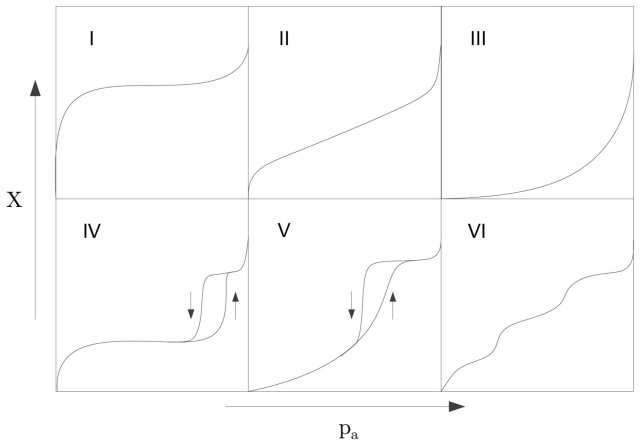

Figure 2.4: Classification of isotherm types [24]

Type I isotherms start with an almost linear slope with rising adsorptive partial pressures, which can be described by *Henry's law*. As pressure increases, the isotherms reach a saturation limit, interpreted as maximum mono-layer loading. The complete isotherm can be described by the *Langmuir model*.

Type II isotherms show a renewed rise at higher partial pressures, after a mono-layer saturation level is reached at low pressures. This indicates either multi-layer adsorption or capillary condensation, whereby the latter is caused by the low saturation vapour pressure in the narrow pores. The *BET equation* describes this type of isotherm.

Type III isotherms have adsorbents, which initially adsorb only little adsorbate at low pressures. This indicates a weak adsorbent-adsorbate interaction. As the loading increases, this repellent interaction subsides and multi-layer adsorption begins, which may turns into condensation. The *Freundlich equation* can be applied for this potential-functional relationship.

Type IV isotherms follow a wave-shaped course with another saturation limit after a renewed rise, due to new accessible pore volume. A hysteresis between adsorption and desorption can be observed, which arises from capillary condensation [25, 26]. The *BET model* can be used again to map this course.

Type V isotherms are s-shaped and reach a saturation loading with increasing partial pressure. It is a combination of type I and III isotherms with hysteresis. The saturation limit corresponds to a state where all pores are completely filled. The *Sips equation*, among others, characterises this type.

Type VI isotherms represent the stepwise adsorption, where the next adsorpt layer is only formed after the previous layer is (almost) complete. Similar curve characteristic can be observed in experiments used to determine adsorption data [27, 28].

In the following, the most relevant isotherm equations are discussed, based on descriptions by Bathen and Breitbach [16] and Kast [16, 23].

Langmuir equation

The Langmuir equation represents a two-parameter formulation for the adsorption equilibrium which can be derived thermodynamically [29].

$$X_{eq} = X_{mon}(T)\,\frac{K_L(T)\,p_a}{1 + K_L(T)\,p_a} \tag{2.6}$$

with p_a as the saturated vapour pressure of the adsorptive and X_{eq} the saturation loading of the adsorbent. For small values of p_a the equation changes into the Henry equation [30, 31], while for high partial pressures it approaches the constant value X_{mon} asymptotically.

$$X_{eq} = K_H(T)\,p_a \tag{2.7}$$

Freundlich equation

In contrast to Langmuir, the Freundlich equation is an empirical two-parameter formulation which can't be derived thermodynamically [32, 33]. Exponent n describes the deviation of the isotherms from the linear relationship of the Henry equation.

$$X_{eq} = K_F(T)\,p_a^{1/n(T)} \tag{2.8}$$

Sips equation

The Sips equation, formed from the combination of the Langmuir and Freundlich equations, considers interactions between the adsorpt molecules and any heterogeneity of the adsorbent [34]. The heterogeneity exponent t describes the non-ideality of the system.

$$X_{eq} = X_{mon}(T)\,\frac{(K_S(T)\,p_a)^{1/t(T)}}{1 + (K_S(T)\,p_a)^{1/t(T)}} \tag{2.9}$$

Other alternative isotherm equations have been developed in order to describe the isotherms of type V, such as the Toth- or Tempkin isotherms as well as the concepts by Frenkel-Hill-Halsey and Volmer or various modifications of Dubinin-Radushkevich approach [16].

Depending on the temperature, however, the isotherms for the same material pairing show different courses. In

general, it is pursued to describe an isotherm field by a closed equation, since section-wise defined functions often deliver worse results in simulations. Empirical equations have been developed for this purpose, but these only provide better results to a limited extent. Today, approachs for predicting isotherms without measurement data are discussed in research, but not yet ready for industry [16]. Databases are available [35], although they are not comprehensive due to the diverse combinations of materials.

2.3.2 Multi-component isotherms

The problem addressed is even more complex for industry-relevant multi-component processes. Several models have been developed to calculate multi-component isotherms from pure isotherms or purely empirically. Here as well, there are often limits, especially in describing the interactions of the adsorptives with each other.

Extension of single-component isotherms:
Many models are based on extending single-component equations. In the following, only the extensions of Langmuir and Freundlich equations for N components are discussed.

Extended Langmuir equation:

$$X_{eq,i}(T) = X_{mon,i}(T)\,\frac{K_{L,i}(T)\,p_{a,i}}{1+\sum_i^N (K_{L,i}(T)\,p_{a,i})} \qquad (2.10)$$

Extended Freundlich equation:

$$X_{eq,i}(T) = k_i(T)\,p_{a,i}\left[\sum_{j=1}^{N}(a_{ij}(T)\,p_j)\right]^{n_i(T)-1} \qquad (2.11)$$

with the empirical competition factor a_{ij}.

It becomes clear that method of expanding single-component isotherms is different for each isotherm type. For further important isotherm models reference is made to Bathen and Breitbach, Kast, and Do [16, 23, 34].

Multi-component models:
More sophisticated models exist that require in-depth knowledge of adsorption thermodynamics. This is why most of them are only of major importance to science. Some common models are:

- Ideal Adsorbed Solution Theory (lAST)
- Real Adsorbed Solution Theory (RAST)
- Simplified Competitive Adsorption (SCA)
- Integral Equation Method (IE)
- Vacancy Solution Model (VSM)
- Multi-Dubinin-Astakhov

Particularly noteworthy is IAST, which forms the fundament for other models and has gained industrial importance. IAST is based on the theory of ideally adsorbed solutions and assumes a chemical equilibrium between gaseous and adsorbed phase. RAST extends IAST to include the interaction between different components. Both methods are iterative procedures and require higher computational effort, which strongly depends on the isotherms' complexity. Various approaches are being pursued to reduce the computational effort, such as the FAST-IAST algorithm does.

A more profound description of these methods can be found in the literature of Do, Myers and Prausnitz, and Steele et al. [34, 36, 37].

2.3.3 Enthalpy of adsorption

Adsorption is an exothermic process. As a rule, no uniform value will be obtained for the enthalpy of adsorption Δh_{ads}, since it is strongly load-dependent. While the maximum value of Δh_{ads} is released during adsorption of the first molecules, this amount is reduced as the loading progresses until adsorption changes to pure condensation Δh_V after a certain layer thickness, as figure 2.5 illustrates.

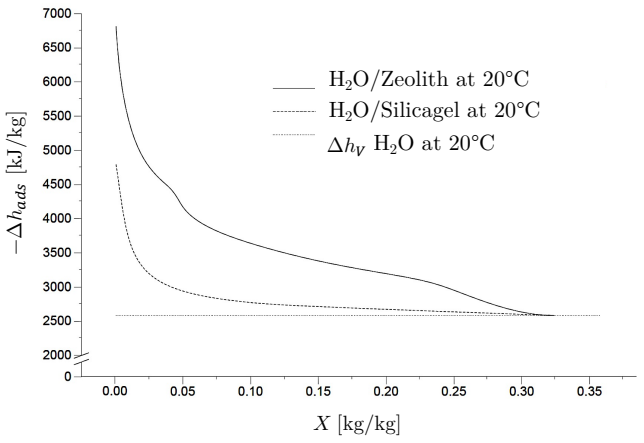

Figure 2.5: Measured Δh_{ads} for different material combinations [38]

If no adsorption data are known, the rough rule of thumb according to equation 2.12 can be used as a first estimation [39]. However, this estimate should be used with some caution, as Δh_V only considers interactions of adsorptive molecules with each other. When paired with different adsorbents, the enthalpy of adsorption can vary greatly for the same adsorptive in use.

$$\Delta h_{ads} = 1.5 - 2\,\Delta h_V \qquad (2.12)$$

With reference to Nuhnen and Janiak [40], approaches to determine the adsorption enthalpy more precisely can basically be done in two ways: experiment-based calculations or molecular simulations. The experimental approach is further divided into a direct and indirect approach: In the direct approach, the adsorption enthalpy is measured directly with a caloric-volumetric system, like in figure 2.5 by Hauer [38]. Nevertheless, these systems are very complex and cost-intensive, which is why the indirect approach is often preferred:

Isosteric method
Since the enthalpy of adsorption is strongly dependent on temperature and loading of the adsorbent, the model developed in this work requires enthalpy values in function of these physical quantities. An accurate prediction can be done, by using the *isosteric method*, which is based on the approach similar to the Clausius-Clapeyron equation:

$$\frac{d(\ln p)}{d(1/T)} = -\frac{\Delta h_{i,ads}}{R} \tag{2.13}$$

$\Delta h_{i,ads}$ can be directly obtained from at least two isotherms measured at two different temperatures [16, 24], which are then fitted with the appropriate models. Afterwards, the isosters are formed from the isotherms, simply presented by using $[X|p_1|p_2]$ data triples from the isotherm fits and plotting $\ln p$ against 1/T, as figure 2.6 shows. The adsorption enthalpy can be determined from the straight line slope of these isosters, according to equation 2.13.

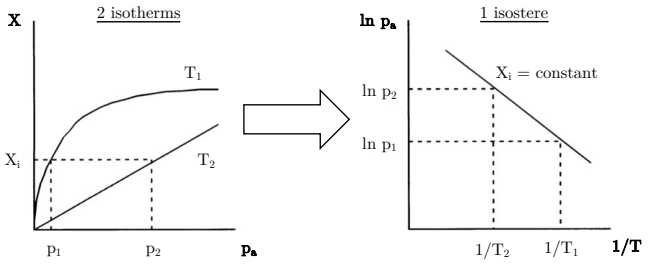

Figure 2.6: Determination of isosters from isotherms [16]

The objective is to provide the corresponding isosters for as many loadings as possible. Computer-assisted, the data sets can be quickly evaluated [40, 41] with

$$\Delta h_{i,ads}(X) = -R \ln\left(\frac{p_2}{p_1}\right) \frac{T_1\, T_2}{T_2 - T_1} \tag{2.14}$$

Following the instructions of Nuhnen and Janiak [40], it is recommended to work with at least three isotherms with temperature differences of about $\Delta T = 10-20K$ to increase the statistical significance. It should be noted that it is not advisable to extrapolate the equilibrium loadings for temperatures outside the isothermal group under consideration. This can be justified by the sensitivity of the interaction energy between adsorbent and adsorptive which results in a significantly worse prediction of equilibrium loading. Instead, the temperature range is to be consciously delimited [40].

2.4 Kinetics

The kinetics describe how fast a physical process reaches its thermodynamic equilibrium. The sorption process is a combination of simultaneous material and heat transport mechanisms, which can take place diffusively and convectively.

2.4.1 Physical adsorption mechanisms

The adsorption process for a adsorptive molecule takes place in seven stages, see figure 2.7. The stages 1 - 4 describe the mass transport and the stages 5 - 7 the heat transport [16]:

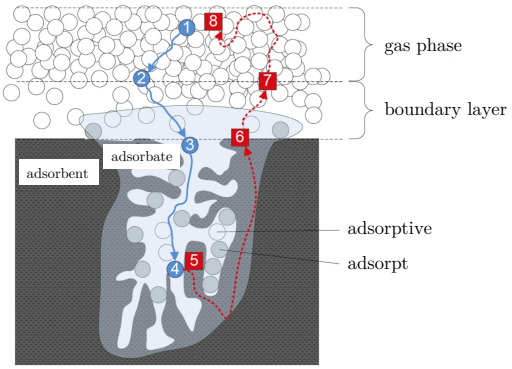

Figure 2.7: Seven stages during adsorption [42]

1. **Mass transport to boundary layer**
   The adsorptive moves first from the fluid bulk phase to the boundary film above the surface of the adsorbent by convective and/or diffusive transfer.
2. **Mass transport through boundary layer**
   The mass transport through the boundary layer occurs by diffusion.
3. **Mass transport in pores of adsorbent**
   In the pores of the adsorbent, different diffusion mechanisms run partly in parallel or one after the other. These complex processes lead to different progressions of the adsorption isotherms, as described in chapter 2.3.1.
4. **Adsorption**
   The proper adsorption in the adsorption process is an exothermic accumulation of the adsorptive to the adsorbent forming an adsorbate.
5. **Energy transport within the adsorbent**
   The resulting adsorption enthalpy is mainly transported by conduction through the adsorbent and to its surface.
6. **Energy transport through boundary layer**
   The heat transport through the boundary layer is diffusive, as is the material transport in stage 2.
7. **Energy transport in the fluid bulk phase**
   The removal of the generated heat occurs in the free fluid by convection and/or conduction, analogue to the mass transport in stage 1.

2.4.2 Transport models

The individual transport mechanisms influence each other and lead to a complex overall process. In principle, the mathematical representation of kinetics is done in two ways: Either all the mechanisms are considered as as a combination of different parallel and/or sequential processes (*heterogeneous model*), where the mathematical description of these mechanisms is done via equations analogous to Fick's law, or the transport process is described as a global mass/heat transport (*homogeneous model*). Both approaches take into account the

mass and energy flows within and at the boundary layer of the adsorbent (stages 1 and 7). Other mechanisms such as mass and energy transport in the gas bulk phase are not directly related to the kinetics of adsorption. Further, diffusive mechanisms within the adsorbent are the dominant resistances of adsorption kinetics, while adsorption itself (stage 4) is fast and its resistance is therefore negligible [16, 23].

In practise, the distinction between the individual diffusive mechanisms is not straightforward. A dominant mechanism and thus a exact physical description of the mass transport is often hardly found. This leads to very cost-intensive studies regarding heterogeneous models, which are rarely sought in industry and accurate kinetics data remain unknown. Thus, the total mass transport between the adsorbent and the fluid phase can be described using a linear driving force (LDF) approach (homogeneous model) [23, 39]:

$$\frac{\partial \psi}{\partial t} = k_{LDF,\psi}\, A_{ssa}\, (\psi_{eq} - \psi) \tag{2.15}$$

In this way, adsorption, diffusion in the pores of the adsorbent and transport through the boundary layer are formulated with a coefficient $k_{LDF,\psi}$, the specific adsorbent particle surface A_{ssa} and a driving gradient of regarded physical quantity $\psi_{eq} - \psi$. In the literature researched, this gradient is often related to the difference between the adsorptive concentration in the gas and in the adsorbent pores [8, 17], but also to the difference between the current adsorbent loading and the equilibrium loading according to the isotherms [43].

2.5 Dynamics

Thermodynamic equilibrium and kinetics are essential for the design and operation of an adsorption plant. These influence each other and together determine the dynamic behaviour of the adsorber, apparent in form of mass transfer zones (MTZ) and breakthrough curves (BTC).

2.5.1 Mass transfer zone

In a fixed bed adsorber, a coupled concentration and loading front moves through a fixed-bed adsorber, as figure 2.8 shows.

During adsorption, the *mass transfer zone* (2) moves through the adsorber in direction of gas flow. The adsorption takes place exclusively in this zone. On the inlet side, the *equilibrium zone* (3), the adsorbent is fully loaded, according to the sorption isotherm. The partial pressure of the adsorptive in the gas phase p_a corresponds to the value of the raw gas at the inlet to the adsorber $p_{a,0}$. On the outlet side, the *equilibrium zone* (1), only the residual load from the previous adsorption and after desorption is present. In this zone, the adsorptive can still almost entirely be adsorbed and the residual partial pressure is at its lowest level. In the beginning of the process, this zone occupies the entire adsorber. At the end of the adsorption cycle, zone 1 is completely displaced by zone 3, i. e. the entire adsorber is fully saturated and the partial pressure of the outlet has risen to the initial value $p_{a,0}$.

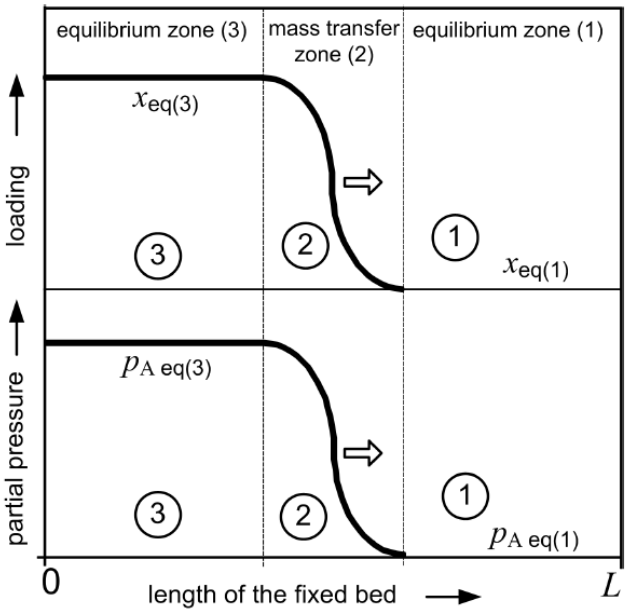

Figure 2.8: Axial adsorptive concentration and adsorbent loading profile through a fixed-bed adsorber [24]

The ideal case described here is usually not found in real adsorbers. The profile shown here only appears after a certain start-up time and start-up distance. This profile usually changes considerably in the course of the adsorption.

2.5.2 Breakthrough curve

Frequently, the migration of the mass transfer zone up to breakthrough is usually determined experimentally in order to estimate the effective height of the adsorbent bed, the achievable total loading and the migration velocity of the mass transfer zone, the adsorption rate.

The breakthrough curve in figure 2.9 represents the time-dependent adsorptive concentration at the outlet, defining the breakthrough time as $t_D = 0.05\, p_a/p_{a,0}$, the half-time value $t_H = 0.5\, p_a/p_{a,0}$ and the total time $t_G = 0.95\, p_a/p_{a,0}$.

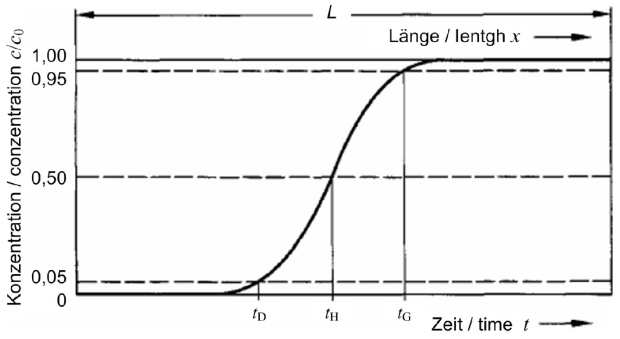

Figure 2.9: Breakthrough curve, adsorptive concentration investigated on the outlet of the adsorber [24]

In order to determine the mentioned design data, breakthrough curves of two different bed depths $H1$ and $H2$ are measured, according to figure 2.10. It is assumed, that the mass transfer zone migrates through the adsorber at a constant velocity with a constant shape. Based on that, the half-value times t_{H1} and t_{H2} of the two bed depths, which corresponds to the adsorptive concentration of $p_a/p_{a,0} = 0.5$, are identified.

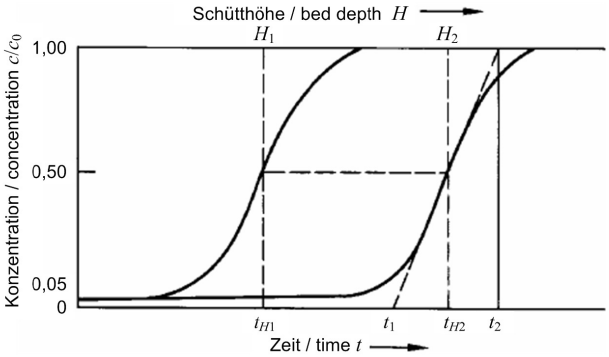

Figure 2.10: Definition of design data from breakthrough curves [24]

The the adsorption rate results in

$$v_{MTZ} = \frac{H_2 - H_1}{t_{H1} - t_{H2}} \tag{2.16}$$

The length of the mass transfer zone H_{MTZ} is calculated by multiplying the adsorption rate with the time interval $t_2 - t_1$, derived from the values of the inflectional tangent laid to the breakthrough curve at $p_a/p_{a,0} = 1$ and $p_a/p_{a,0} = 0$:

$$H_{MTZ} = v_{MTZ}\,(t_2 - t_1) \tag{2.17}$$

The theoretically useable bed depth H_{MTZ} up to the breakthrough of the adsorber can be derived from the total bed depth H as follows

$$H_{th} = H - 0.5\,H_{MTZ} \tag{2.18}$$

The loading X taken up by the mass m_s of the solid adsorbent at any point of time t is represented by the following equation

$$X(t) = \frac{\dot{V}}{m_s}\,\frac{M_a}{RT}\int_0^t (p_{a,0} - p_a)\,dt \tag{2.19}$$

2.5.3 Influences on dynamics

Adsorption capacity, selectivity, release and transfer of heat as well as the sorption rate, inlet concentration and gas velocity play a key role during the adsorption process and influence the position and shape of the breakthrough curve significantly.

Various macroscopic, mesoscopic and microscopic parameters influence the shape and position of breakthrough curves, as summarised in figure 2.11 and table 2.2.

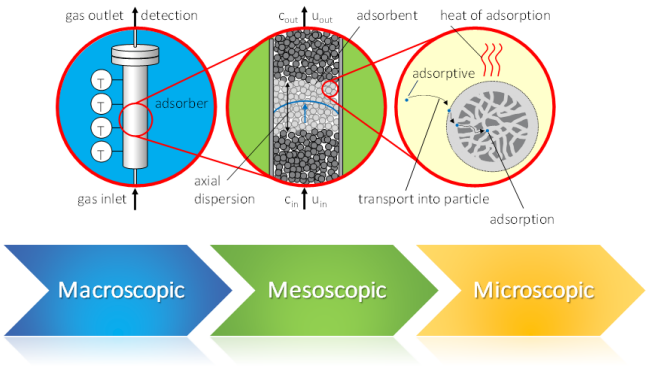

Figure 2.11: Different scales which influence the adsorption under dynamic conditions [44]

Table 2.2: Influences on different scales

Macroscopic influences	**Mesoscopic influences**	**Microscopic influences**
adsorber size	fixed bed type	pore structure
adsorber form	bed porosity	surface chemistry
gas velocity	adsorbent shape/size	adsorptive accessibility

Here the five most important parameter and their impact are summarized [44]:

- The **adsorption capacity** has a big impact on the position of the breakthrough curve. By increasing of the capacity, more adsorptive will be adsorbed. The breakthrough curve will be shifted to the right and longer breakthrough times occur. This is not the case if the kinetics is too slow and a spontaneous breakthrough occurs.
- The **adsorption kinetics** affect the shape of the breakthrough curve. For faster kinetics the breakthrough curve becomes steeper and the mass transfer zone will be smaller. However, fast mass transfer leads to short local equilibrium times and therefore for lower loading of the adsorbent.
- In some cases these two advantages will be compensated by the **release of adsorption heat**. An increasing temperature leads to a flatter, more asymmetric breakthrough curve and the mass transfer zone will expanse.
- A fourth parameter is the **axial dispersion**, which is responsible for a broadening of the mass transfer zone. This parameter is also responsible for an increasing asymmetric character of the breakthrough curves.
- The **curvature of the isotherm** can have effects on the shape of breakthrough curves as well. A type 1 isotherm leads to smaller mass transfer zones during adsorption. The desorption curve is broadened in such cases. The opposite can be observed for type 3 and type 5 isotherms.

2.6 Characterisation of adsorbents

Typical technical adsorbents are activated carbon, activated alumina, silica gel or molecular sieves. Generally, five groups of adsorbents are distinguished:

- carbonaceous adsorbents
- oxidic adsorbents
- polymer adsorbents
- mixed adsorbents
- metal-organic frameworks (MOF)

Major requirements on adsorbents are:

- high adsorption capacity (size of inner surface)
- good accessibility of the surface for adsorptives
- sufficient selectivity towards one gas component
- high robustness (thermal and chemical stability)
- favourable desorption characteristics
- low bed pressure drop
- low price

For the characterisation of adsorbents, specifications are given in particular on: particle size distribution, densities, porosities, internal or specific surfaces and pore radius distribution. The particle and pore sizes are differentiated between modal values, mean values and size ranges. In this work, mean values are taken into account. Important adsorbent parameters relevant for modelling in this work are:

- net density ρ_n, resp. solid material density, as ratio of particle mass m_p and solid volume V_{solid}:

$$\rho_n = \frac{m_p}{V_{solid}} \tag{2.20}$$

- gross density ρ_g, resp. particle density, as ratio of m_p and the sum of V_{solid} and pore volume V_{pore}:

$$\rho_g = \frac{m_p}{V_p} = \frac{m_p}{V_{pore} + V_{solid}} \tag{2.21}$$

- bed density ρ_{bed}, as ratio of total mass of adsorbent bed m_{bed} within adsorber column volume $V_{adsober}$, including the pore volume:

$$\rho_{bed} = \frac{m_{bed}}{V_{adsober}} \tag{2.22}$$

- particle porosity ε_p:

$$\varepsilon_p = 1 - \frac{\rho_g}{\rho_n} \tag{2.23}$$

- bed porosity ε_{bed}, or void fraction:

$$\varepsilon_{bed} = 1 - \frac{\rho_{bed}}{\rho_g} \tag{2.24}$$

- volume specific surface area of adsorbent A_{ssa} as ratio of particle surface area A_p and V_p:

$$A_{ssa} = \frac{A_p}{V_p} \tag{2.25}$$

Table 2.3 gives an exemplary overview on the wide range of characteristics of different activated carbons (powders, granules, pressed forms).

Table 2.3: Parameter ranges of different activated carbons [16]

Parameter	Symbol	Unit	Value
net density	ρ_n	kg/m^3	1880 - 2100
gross density	ρ_g	kg/m^3	440 - 850
bed density	ρ_{bed}	kg/m^3	250 - 550
particle porosity	ε_p	–	0.45 - 0.77
particle diameter Ø	d_p	mm	0.1 - 4
pore diameter	d_{pore}	nm	0.3 - X000
sp. pore volume	v_p	cm^3/g	0.7 - 1.5
sp. inner surface	A_{inner}	m^2/g	500 - 1800
tortuosity factor	τ	–	7
sp. heat capacity	c_p	kJ/(kg K)	0.76 - 0.92
th. conductivity	λ	W/(m K)	0.65 - 0.85

The size, shape and structure of the adsorbent particles influence the mass transfer between the fluid and solid phases, the selectivity and accessibility of adsorptives or the pressure loss when flowing through the adsorbent bed. Thereby, the choice and design of the adsorbents frequently encounters optimisation problems, for example regarding size or inner surface:

The smaller the particles are , the shorter the diffusion paths and the greater the mass transfer get, but this increases pressure loss across the bed.

High adsorption capacities require large inner surfaces. But since inner surface is inversely proportional to pore diameter, the molecular size of the adsorptive is a lower limit for the pore diameter, otherwise the molecules can't diffuse into pores.

2.7 Process and desorption methods

Adsorption plants with fixed beds are operated discontinuously. This means that at least two columns are operated in parallel. As the flow diagram in figure 2.12 shows, one column takes up the raw gas and adsorbs the components, while the other column is regenerated, resp. it desorbs.

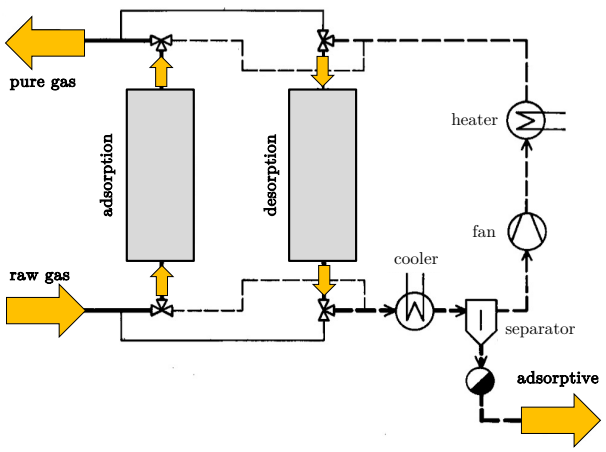

Figure 2.12: Flow diagram of a discontinuously operating adsorption plant with two fixed beds.

Desorption is the most energy-intensive and thus most expensive process step in adsorption plants. While adsorption is carried out at high pressures and low temperatures, desorption is done at low pressures and high temperatures. Again, a thermodynamic equilibrium favourable for this is thus imposed from the outside. In principle, this can be achieved in three ways:

- Temperature Swing Adsorption (TSA)
  - increase of temperature
    → reduction of equilibrium partial pressure
- Pressure Swing Adsorption (PSA)
  - Lowering of system pressure
    → reduction of adsorptive partial pressure
- Concentration Swing Adsorption (CSA)
  - change of gas mixture composition
    → reduction of adsorptive partial pressure

These three mechanisms are clarified in the isothermal diagram of figure 2.13. In addition to these "pure" procedures, there are usually also mixed procedures applied, e. g. purge with hot gas.

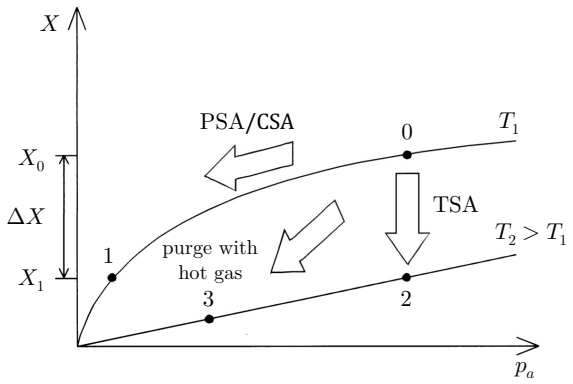

Figure 2.13: Principles of desorption methods

3 Requirements specification

In coopartion with the *Research Group SORPTION*, the requirements for the mathematical-physical model of fixed bed adsorber column and the software with its graphical user interface were specified. The requirements specification are devided into sections "Modelling / Simulation" and "Software / GUI".

The requirements were categorised in terms of

- BC: boundary conditions
- FC: functional conditions
- QC: quality conditions

and prioritised according to their importance into

- F: fixed requirements
- D: desired requirements
- O: optional requirements

3.1 Modelling / Simulation

The mathematical-physical model forms the core of the simulations carried out in Python. The model should represent the process as accurate as possible and provide the desired data and simulation results, which are further processed in the software. Therefore, more demanding requirements are placed on the modelling.

Table 3.1: Requirements on modelling

Requirements	**Prio.**	**Cat.**
Modelling, Objective variables:		
adsorbent loadings X_{tot}, X_i	F	QC
adsorptive concentrations $\rho_{a,i}$	F	FC
adsorbent temperature T_s	F	FC
gas temperature T_g	F	FC
pressures p_{tot}, p_i	F	FC
adsorbed masses $m_{ads,tot}, m_{ads,i}$	F	FC
other resolved quantities	D	FC
internally calculated variables	O	FC
performance & efficiency calculations	D	FC
time & space resolved dynamic model	F	FC
material and energy balances	F	BC
momentum balance	F	BC
pressure loss considered	F	BC
macroscopic / mesoscopic model scale	F	BC
Process:		
fixed bed axial adsorber	F	BC
multi-component adsorption (2 ads.)	F	BC
carrier gas behaves inertly	F	BC
non-isothermal adsorption	F	BC
diabatic process	F	BC
axial dispersed plug flow	F	BC
desorption method: TSA	F	FC
desorption method: PSA	F	FC
desorption method: CSA	F	FC
desorption method: hot gas purge	F	FC
Geometry:		
adsorber: cylindrical, constant	F	BC
no influence of installed components	F	BC
radial effects neglected (1D model)	F	BC
...		
Material:		
homogeneous adsorber bed	F	BC
homogeneous adsorbent particles	F	BC
gas phase subject to ideal gas law	F	BC
homogeneous gas phase	F	BC
gas phase within pores neglected	F	BC
T-dependence of main phys. quantities	D	QC
p-dependence of main phys. quantities	D	QC
Equilibrium, Kinetics:		
equilibrium loading base: isotherms	F	QC
isotherm base: measured data	F	QC
enthalpy of ads.: isosteric method	F	QC
mass transport: homogeneous model	F	QC
heat transport: homogeneous model	F	QC
LDF coeff. is derived from resistances	D	QC

3.2 Software / GUI

The model is discretised and implemented in Python. The entire software forms the shell around the model. It is intended to support the user in entering parameters, preparing important thermodynamic and material data and exporting the simulation data and evaluating the results graphically. Suitable functions are equipped with GUI elements with regard to inputs, outputs and user interactions.

Table 3.2: Requirements on software

Requirements	**Prio.**	**Cat.**
General:		
user language: English	F	BC
implementation software: Python	F	BC
simple but consistent user interface	D	QC
easy to operate	F	QC
quick in response	F	QC
physical mode: phys. correct use cases	F	QC
custom mode: free parameter setting	O	FC
SW as a design & visualisation tool	F	BC
SW is no optimisation tool	F	BC
GUI - attractive graphical UI	F	QC
GUI as integral cockpit window	D	QC
Step-by-Step design/calc. guide	D	QC
autonom. guidance for user errors	O	FC
Inputs:		
const. initial and boundary conditions	F	FC
process times (ads./des.)	F	FC
transient boundary conditions	O	FC
adsorber dimesnion incl. wall	F	FC
adsorbent properties	F	FC
gas mixture composition	F	FC
adsorptive properties	F	FC
carrier / bulk gas properties	F	FC
equilibrium data: measurement data	F	FC
no direct enthalpy data user input	F	FC
desorption method: inlet B.C.	F	FC
economic parameters	D	FC
simulation parameters	F	FC
Outputs:		
objective variables at time and position	F	FC
mass transfer zone along adsorber bed	F	FC
heat waves along adsorber bed	F	FC
breakthrough curve at outlet	F	FC
adsorbed amount	F	FC
isotherm group in function of loading	F	FC
bed temperatures at defined positions	F	FC
energetic & economic key figures	D	FC
data store of objective variables	F	FC
data store of input parameters	D	FC
data store of internal variables	O	FC

4 Software concept

This chapter presents the concept for the user software, based on the defined requirements in the previous chapter.

It is shown which benefits the software should fulfil on the basis of a user journey respectively a design procedure of an engineer. Further, the defined steps are explained in more detail with regard to what the user is intended to do and how the software is supporting. Next, the software structure is pointed out. Finally, the required user inputs are defined and it is shown how the user interface can be designed.

4.1 User journey

When designing a process, an engineer goes through several stages. For adsorption processes in particular, the first step is to determine the boundary conditions, e. g. what is the composition and volume flow of the raw gas and what requirements must be met by the pure gas. Furthermore, the selection of the appropriate material pairing adsorptive-adsorbent as well as the dimensioning of the fixed-bed adsorber have a significant influence on the process performance. Data on isotherms and adsorption enthalpies needed for the modelling of equilibria is taken from literature or databases if available or determined experimentally for the specific material pairing.

Whether technical, energetic and economic requirements are met can't be answered with sufficient accuracy using simple shortcut methods. In addition, the design procedure and optimisation is iterative and is carried out by the engineer himself. Depending on the extent of parameter variation, the achievement of the final design can be greatly delayed. Therefore, accurate calculations of the adsorber dynamics are required which can be carried out quickly and easily. The main benefit of the software should be to enable designing and comparing of process variants in a short time without the engineer having to deal with the modelling and simulation of the process (equilibria, kinetics). On this basis, the five main design steps are defined, as figure 4.1 shows.

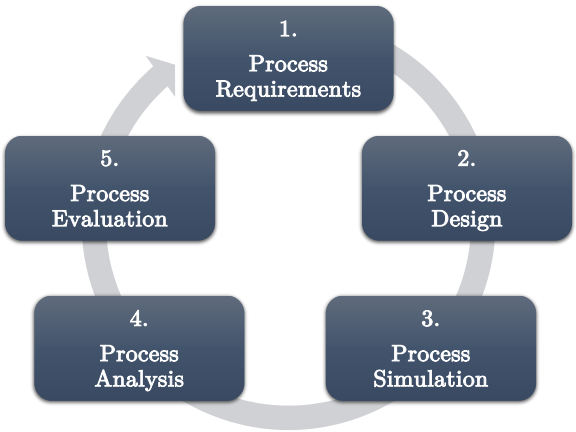

Figure 4.1: The five process design steps

4.2 Design steps

The defined design steps are explained in more detail in the following table with regard to their contents and objectives as well as the processes that are carried out by the user and the software.

Table 4.1: The five process design steps described regarding its contents/goals and procedures performed by user and software

Step	Content / Goals	User/Software Procedures
1. Process Requirements	- Clarification of requirements and boundary conditions	1. Inlet conditions of raw gas 2. Gas components properties 3. Required outlet conditions of pure gas
2. Process Design	- Adsorbent selection - Adsorber design - Choice of desorption method - Cost parameters	1. Selection of material pairing 2. Import of sorption isotherm measurement data 3. Definition of additional adsorbent data 4. Dimensioning of adsorber column 5. Selection of desorption method 6. Definition of cost parameters (investment and operating)
3. Process Simulation	- Modelling of isotherms - Modelling of enthalpy of adsorption - Definition of initial conditions - Simulation	1. Selection of isotherm models 2. Fitting with isotherm models (SW calculates model parameters) 3. Calculation of isosteric enthalpy in function of loading 4. Fitting of isosteric enthalpy model (SW calculates model parameters) 5. Definition of initial conditions within adsorber 6. Simulation execution
4. Process Analysis	- Mass transfer zones - Heat waves - Breakthrough curves - Ad-/desorbed mass - Bed temperatures	1. Visualisation of mass transfer zones and heat waves 2. Visualisation of breakthrough curves 3. Visualisation of ad-/desorbed mass 4. Visualisation of bed temperatures 5. Interactions on time-based process variables
5. Process Evaluation	- Feasibility - Process performance - Energetic key figures - Economic key figures	1. Feasibility based on pre-defined duration of total process, sub-processes 2. Process performance: - productivity - purity - recovery 3. Energy: - absolute and specific energy demand - energetic separation efficiency 4. Economy: - absolute costs (total, per sub-process) - levelised costs of separation

The actions performed by the user during these design steps are:

1. Definition of process requirements
2. Selection of the adsorptive-adsorbent pairing

3. Search for material characteristic data
4. Search for isotherm measurement data
5. Input of process & material parameters
6. Input of measurement data
7. Start simulation
8. Analysis of results
9. Evaluation of simulated process

The actions and functions of the software are explained by means of a solution algorithm:

1. Reading of input parameter and measurement data
2. Fitting of isotherms $X(p_a, T_s)$ with models defined by user
3. Calculation and mathematical fitting of adsorption enthalpy $\Delta h_{ads}(X)$
4. Discretisation in m time steps and n adsorber volume elements
5. Solution of conservation equations for each element and time step:
   - Saving data from previous time step
   - Calculation of equilibrium loading by interpolation between isotherms
   - Calculation of enthalpy of adsorption based on the current loading
   - Calculation of the material and heat transfer coefficients
   - Solution of the PDEs
   - Recalculation of remaining state variables based on ideal gas law
   - Updating objective and internal variables
6. Export of simulation data
7. Generation of diagrams for objective variables, MTZ and breakthrough curve
8. Calculation of key figures

4.3 Software structure

The structure of the software is defined by four levels:

- **System:** User interface/GUI, input/output widgets
- **Architecture:** Functional order of modules and logical embedding in user interface.
- **Modules:** Inputs, outputs, graphs, adsorber Model, modelling isotherms, modelling enthalpy, equilibria functions, kinetics functions, etc.
- **Code:** Code structure for Modules and architecture interfaces

The following V-model in figure 4.2 shows the relationship between these software levels and the development phases, and explains how the validation and verification of each stage are organised.

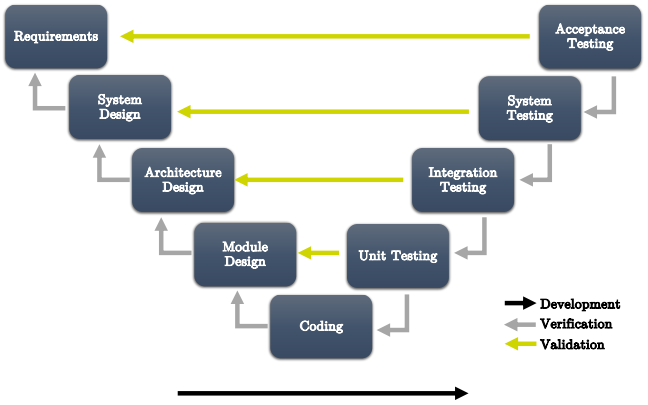

Figure 4.2: V-model showing the development stages with verification and validation relationships between each stages and software levels

4.4 Defined inputs

During concept development, the most important input parameters were fixed, as listed in table 4.2:

Table 4.2: Defined user input parameters

Parameter	Symbol	Unit
Adsorption column data		
length	L	m
inner diameter	d	m
wall thickness	s_w	m
sp. heat capacity	$c_{p,w}$	J/(kg K)
th. conductivity	λ_w	W/(m K)
Adsorbent properties		
adsorbent type (name)	–	–
bed density	ρ_{bed}	kg/m^3
gross density particle	ρ_g	kg/m^3
net density particle	ρ_n	kg/m^3
particle diameter	d_p	m
pore diameter	d_{pore}	m
tortuosity factor	τ	–
sp. heat capacity	$c_{p,s}$	J/(kg K)
th. conductivity	λ_s	W/(m K)
Adsorptive(s) properties		
adsorptive type (name)	–	–
molar mass	M_a	kg/mol
sp. heat capacity	$c_{p,a}$	J/(kg K)
collision diameter	σ_a	Å
interaction potential	ε_a/k_B	K
Bulk gas properties		
bulk gas type (name)	–	–
molar mass	M_b	kg/mol
sp. heat capacity	$c_{p,b}$	J/(kg K)
collision diameter	σ_b	Å
interaction potential	ε_b/k_B	K
Process parameters		
volume flow (std.)	$\dot{V}$	L/min
system pressure	p_{tot}	Pa
mole fractions adsorptives	$x_{a,i,in}$	–
- or concentrations	$\rho_{a,i,in}$	kg/m^3
inlet gas temperature	$T_{g,in}$	K
Initial conditions adsorber		
mole fractions adsorptives	$x_{a,i,0}$	–
- or concentrations	$\rho_{a,i,0}$	kg/m^3
gas and solid temperature	T_0	K
Simulation parameters		
simulated process time	$t_{process}$	s
time steps	Δt	s
number of discretized elements	n	–

4.5 User interfaces

The software is implemented exclusively in Python with additional open source function packages such as "pyside" for graphical interfaces.

In principle, the graphic elements can be arranged in such a way that individual pop-up windows appear one after the other when the programme is executed, like shown in figure 4.3, or that all elements are integrated in one cockpit window according to figure 4.4 .

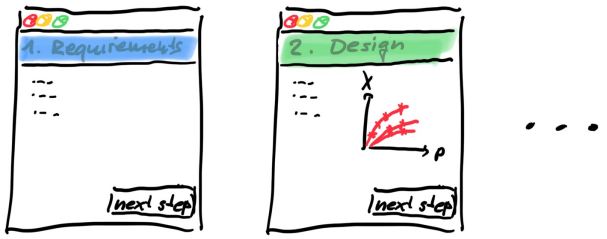

Figure 4.3: GUI variant with successive pop-up windows

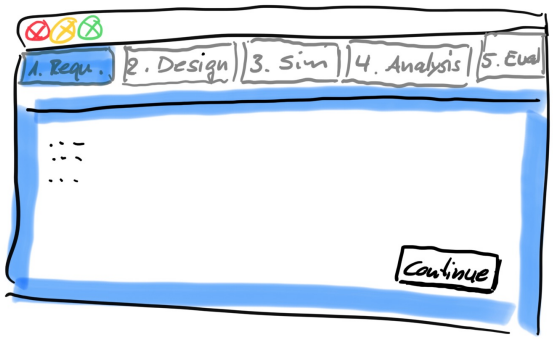

Figure 4.4: GUI variant where all graphical elements are intergrated within a cockpit window

The advantage of the first variant is the simpler implementation. This greatly limits the flexibility of the programme, because the sequence of interaction is strictly predetermined. The second variant is advantageous in terms of a clearer simultaneous display of all elements, which allows better interaction with the programme by the user. However, the implementation in code is more complex.

To achieve a compromise between implementation effort and user-friendliness of the programme, it was decided that the software would have a suitable combination of input windows, Python terminal prints and graphical output windows with possible user interactions, which are mainly realised as pop-up windows. This is to be created in an iterative manner during development.

5 Mathematical model

The developed mathematical-physical model for multi-component adsorption is presented here. Key assumptions, modelled components and their interrelationships within the overall model are discussed, starting with material, energy and momentum balancing, deriving of necessary differential equations, then understanding initial and boundary conditions and finally explaining how mass and heat transport as well as axial dispersion are modelled.

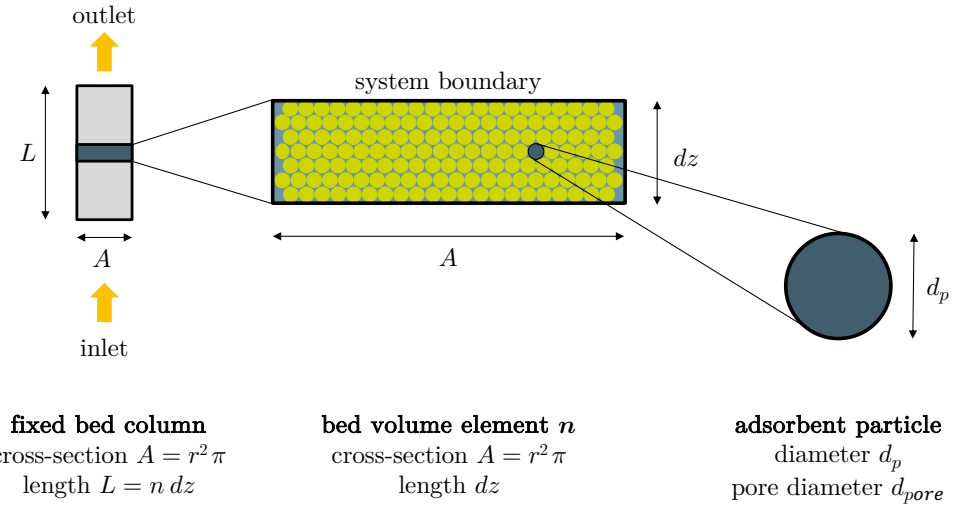

Figure 5.1: Balance area of adsorber bed volume element

5.1 Overview

The 1D model follows the kinetic approach and is derived on a mesoscopic scale. The material, energy and momentum balances are carried out on a cell i. e. volume element of the adsorber, as figure 5.1 illustrates whereby the characteristic geometric parameters for adsorber bed and adsorbent particle are indicated. Further parameters used are explained in chapter 2.6.

For the representation of general multi-component adsorption, a material balance is required for each adsorptive i both in the gas and solid phases, while for each phase one energy balance in total is needed. Further, one momentum balance is solved within the gas phase.

- solid phase material balance i
- gas phase material balance i
- solid phase energy balance
- gas phase energy balance
- gas phase momentum balance

5.2 Model assumptions

The model is based on the following assumptions:

1. A non-isothermal multi-component adsorption is modelled.
2. Pressure loss along adsorber bed length is considered.
3. The process is diabatic with constant column wall temperature.
4. The bulk gas, resp. carrier gas, is assumed to behave inertly, why its mass flow is set constant.
5. Heat flows to column wall are summarised within gas phase, since bed void fraction next to the column wall aims for 1 [23].
6. The gas phase is homogeneous and subject to the ideal gas law $p = \sum_i p_i = \sum_i (\rho_i\, R_i\, T_g)$.
7. Radial effects such as velocity-, temperature- or concentration gradients are neglected.
8. The adsorber geometry is cylindrical and constant.
9. The geometry of adsorbent particles is described as equivalent spheres regarding form and size and the material structure is homogeneous.
10. The unloaded adsorbent bed is regarded as a homogeneous system.
11. Heat capacities of adsorbent $c_{p,s}$, adsorptives $c_{p,a,i}$ and bulk gas $c_{p,b}$ are chosen to be constant.
12. The gas phase within the adsorbent pores is neglected since a gross density ρ_g is defined.
13. A homogeneous approach is adopted for heat and mass transport.
14. The conductive heat transport of solid phase is subsumed in the gas phase [23, 45].
15. Within the adsorbate, the adsorbt is considered to be part of the solid phase and therefore is taken into account in the corresponding storage term. This also enables the definition of an adsorptive enthalpy flow from the gas phase to the solid phase.

5.3 Conservation equations

In the following, the required balance equations are set up for the general case of multi-component adsorption. From these the partial differential equations are derived.

5.3.1 Solid phase material balance i

During adsorption, the adsorptive migrates from the gas phase into the solid phase and is adsorbed there, according to figure 5.2.

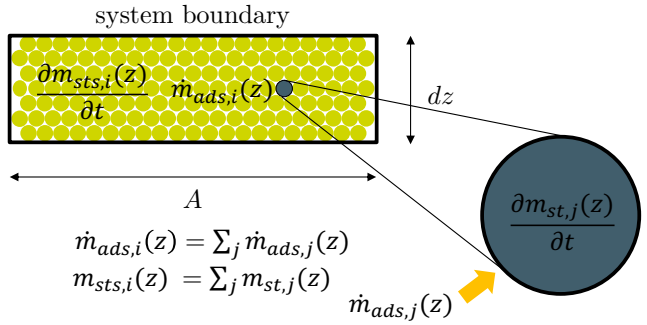

Figure 5.2: Solid phase material balance

The transient storage term is opposed to the adsorption mass transport term by

$$\frac{\partial\, m_{sts,i}(z)}{\partial t} = \dot{m}_{ads,i}(z) \tag{5.1}$$

The storage term is replaced by the adsorbent loading X_i, which is based on the constant solid adsorbent mass m_s. The adsorbent mass is further expressed by the volume element $dV = A\, dz$, the bed porosity ε_{bed} and the gross density of the adsorbent particle ρ_g.

$$\frac{\partial\, m_{sts,i}}{\partial t} = m_s \frac{\partial X_i}{\partial t} = \rho_g\,(1-\varepsilon_{bed})\, A\, dz \frac{\partial X_i}{\partial t} \tag{5.2}$$

The adsorption mass flow rate is formulated with the overall mass transfer coefficient $k_{m,i}$, the volume specific surface area A_{ssa} of the adsorbent and the driving loading difference $(X_{eq,i} - X_i)$ within the adsorbent. The loading difference results from the current loading X_i and the equilibrium loading $X_{eq,i}(T_s, p_{a,i})$, which depends on present temperature of the solid phase T_s and partial pressure of the adsorptive $p_{a,i}$ in the gas phase.

$$\dot{m}_{ads,i} = k_{m,i}\, A_{ssa}\, \rho_g\,(1-\varepsilon_{bed})\, A\, dz\,(X_{eq,i} - X_i) \tag{5.3}$$

Inserting equations 5.2 and 5.3 into equation 5.1 results in the first differential equation, which follows the homogeneous approach described in chapter 2.4.2.

$$\frac{\partial X_i}{\partial t} = k_{m,i}\, A_{ssa}\,(X_{eq,i} - X_i) \tag{5.4}$$

5.3.2 Gas phase material balance i

The gas phase material balance consists of four terms:

- storage term $\frac{\partial\, m_{stg,i}}{\partial t}$
- convective axial material flow $\dot{m}_{c,i}$
- diffusive axial material flow $\dot{m}_{d,i}$
- adsorption mass flow $\dot{m}_{ads,i}$

The overall balance is derived as

$$\frac{\partial\, m_{stg,i}(z)}{\partial t} = -\frac{\partial\, \dot{m}_{c,i}}{\partial z}\, dz - \frac{\partial\, \dot{m}_{d,i}}{\partial z}\, dz - \dot{m}_{ads,i}(z) \tag{5.5}$$

with the following expression for the in- and out-flowing transport terms, when a Taylor series expansion is carried out and is terminated after the second term.

$$-\frac{\partial\, \dot{m}_i}{\partial z}\, dz \approx \dot{m}_i(z) - \dot{m}_i(z + dz) \tag{5.6}$$

Figure 5.3 explains the balancing of the four terms and shows in particular the single in- and out-flowing transport terms of the convective and dispersive material flows:

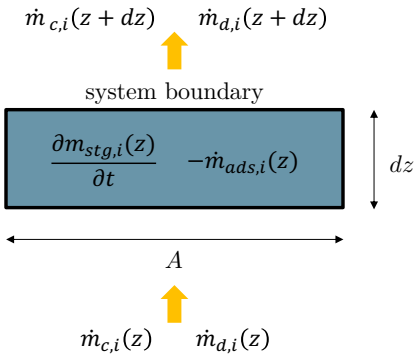

Figure 5.3: Gas phase material balance

The storage term is defined by

$$\frac{\partial\, m_{stg,i}}{\partial t} = \varepsilon_{bed}\, A\, dz \frac{\partial\, \rho_{a,i}}{\partial t} \tag{5.7}$$

The convection term varies along the bed as both the partial density $\rho_{a,i}$, or mass concentration, and the volume flow rate $\dot{V}$ change due to the adsorption and the resulting temperature increase. The following expression results:

$$\frac{\partial\, \dot{m}_{c,i}}{\partial z} = \frac{\partial}{\partial z}\,(\rho_{a,i}\, \dot{V}) = \dot{V}\, \frac{\partial\, \rho_{a,i}}{\partial z} + \rho_{a,i}\, \frac{\partial\, \dot{V}}{\partial z} \tag{5.8}$$

The diffusion term is defined with the axial diffusion coefficient $D_{ax,i}$, the column cross-section A and the gradient $\frac{\partial^2 \rho_{a,i}}{\partial z^2}$.

$$\frac{\partial\, \dot{m}_{d,i}}{\partial z} = -D_{ax,i}\, \varepsilon_{bed}\, A\, \frac{\partial^2 \rho_{a,i}}{\partial z^2} \tag{5.9}$$

The adsorption mass flow forms the important exchange term between gas and solid phase. It is formulated analogously to the solid phase material balance in chapter 5.3.1.

The insertion of equations 5.3, 5.7, 5.8 and 5.9 into equation 5.5 leads to the second differential equation:

$$\begin{aligned}\frac{\partial \rho_{a,i}}{\partial t} =& -\frac{1}{\varepsilon_{bed} A}\frac{\partial (\rho_{a,i}\dot{V})}{\partial z} + D_{ax,i}\frac{\partial^2 \rho_{a,i}}{\partial z^2} \\ & - \rho_g \frac{1-\varepsilon_{bed}}{\varepsilon_{bed}} k_{m,i} A_{ssa} (X_{eq,i} - X_i)\end{aligned} \tag{5.10}$$

5.3.3 Solid phase energy balance

The energy balance for the solid phase described by equation 5.11 comprises the storage term $\frac{\partial E_{sts}}{\partial t}$, the sensible heat flow term $\dot{Q}_{sen}$ for the heat transport between the adsorbent and the flowing gas, and the adsorption enthalpy flow $\dot{H}_{ads}$, as the sum of all adsorptives' flows $\dot{H}_{ads,i}$. Figure 5.4 clarifies the energy balance on the volume element.

$$\frac{\partial E_{sts}(z)}{\partial t} = -\dot{Q}_{sen}(z) + \dot{H}_{ads}(z) \tag{5.11}$$

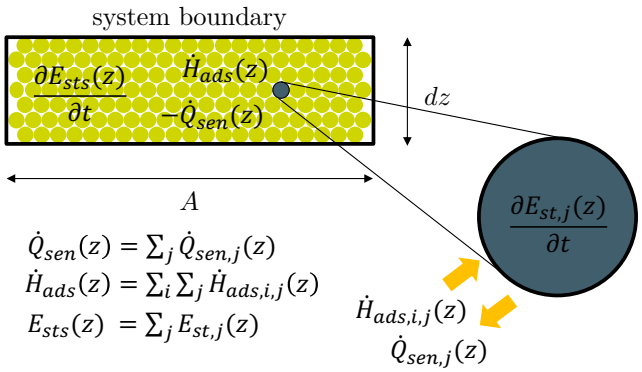

Figure 5.4: Solid phase energy balance

Considering the storage term, it is defined to consist of two parts: the heat storages by the solid adsorbent (s) and by the adsorpts (a,i). The wall is not content of solid phase. The following equation sums up these parts as

$$\frac{\partial E_{sts}}{\partial t} = \frac{\partial}{\partial t}((m_s c_{p,s} + \sum_i (m_{a,i} c_{p,a,i}))T_s) \tag{5.12}$$

with the mass of the individual parts

$$m_s = \rho_g V_s = \rho_g (1-\varepsilon_{bed}) A\, dz \tag{5.13}$$

$$m_{a,i} = X_i m_s = X_i \rho_g (1-\varepsilon_{bed}) A\, dz \tag{5.14}$$

Inserting equations 5.13 and 5.14 into equation 5.12, results in

$$\begin{aligned}\frac{\partial E_{sts}}{\partial t} =& \rho_g (1-\varepsilon_{bed}) A\, dz (c_{p,s} + \sum_i (X_i c_{p,a,i}))\frac{\partial T_s}{\partial t} \\ & + \rho_g (1-\varepsilon_{bed}) A\, dz\, T_s \sum_i \left(c_{p,a,i}\frac{\partial X_i}{\partial t}\right)\end{aligned} \tag{5.15}$$

The sensible heat flow from the solid to the gas phase is regarded as an overall heat transfer k_h at the specific surface area of the particle A_{ssa} within the volume element $dV = A\, dz$:

$$\dot{Q}_{sen} = k_h A_{ssa} (1-\varepsilon_{bed}) A\, dz (T_s - T_g) \tag{5.16}$$

The adsorption enthalpy flow in equation 5.17 mainly describes the exothermic characteristic of the adsorption process, based on the adsorptive-adsorbent interaction energy, the (isosteric) enthalpy of adsorption $\Delta h_{ads,i}(X_i)$, depending on the relevant adsorbent loading X_i. Its value is negative, since it is defined as the energy which is released from the adsorbate [40]. Moreover, an enthalpy flow occurs to the adsorbent $h_{a,i}$, due to the adsorption mass flow $\dot{m}_{ads,i}$ from equation 5.3, at gas temperature T_g.

$$\dot{H}_{ads} = \Delta\dot{H}_{ads} + \dot{H}_a = \sum_i ((-\Delta h_{ads,i} + c_{p,a,i} T_g)\dot{m}_{ads,i}) \tag{5.17}$$

By substituting the terms in the balance equation 5.11 with the equations 5.15, 5.16 and 5.17, and considering again the first differential equation 5.4, the third differential equation is obtained:

$$\begin{aligned}\frac{\partial T_s}{\partial t} =& \frac{1}{c_{p,s} + \sum_i (X_i c_{p,a,i})}\Big[-\frac{k_h A_{ssa}}{\rho_g}(T_s - T_g) \\ & + \sum_i \left(k_{m,i} A_{ssa} (-\Delta h_{ads,i} + c_{p,a,i}(T_g - T_s))(X_{eq,i} - X_i)\right)\Big]\end{aligned} \tag{5.18}$$

5.3.4 Gas phase energy balance

The gas phase energy balance consists of six terms in general:

- storage term $\frac{\partial E_{stg}}{\partial t}$
- convective axial enthalpy flow $\dot{H}_c$
- diffusive axial enthalpy flow $\dot{H}_d$
- adsorptive enthalpy flow $\dot{H}_a$
- heat flow between solid and gas phase $\dot{Q}_{sen}$
- heat flow to column wall $\dot{Q}_w$

The overall energy balance is

$$\begin{aligned}\frac{\partial E_{stg}(z)}{\partial t} =& -\frac{\partial \dot{H}_c}{\partial z} dz - \frac{\partial \dot{H}_d}{\partial z} dz \\ & - \dot{H}_a(z) + \dot{Q}_{sen}(z) - \dot{Q}_w(z)\end{aligned} \tag{5.19}$$

The axial transport terms are again expressed following the equation 5.6. Figure 5.5 explains the balancing and shows in particular the single in- and out-flowing transport terms of the convective and dispersive enthalpy flows:

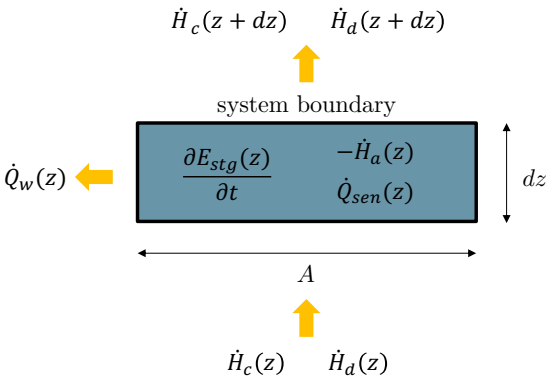

Figure 5.5: Gas phase energy balance

The storage term is composed of the proportions for the bulk gas and the adsorptive

$$\frac{\partial E_{st,g}}{\partial t} = \frac{\partial}{\partial t}((m_b\, c_{p,b} + \sum_i (m_{a,i}\, c_{p,a,i}))\, T_g) \tag{5.20}$$

with the mass of the individual gas fractions of the bulk gas (b) and the adsorptive (a)

$$m_b = \rho_b\, dV_g = \rho_b\, \varepsilon_{bed}\, A\, dz \tag{5.21}$$

$$m_{a,i} = \rho_{a,i}\, dV_g = \rho_{a,i}\, \varepsilon_{bed}\, A\, dz \tag{5.22}$$

The bulk gas is assumed to not participate in the adsorption and thus remains constant. Inserting equations 5.21 and 5.22 into equation 5.20, results in:

$$\begin{aligned}\frac{\partial E_{st,g}}{\partial t} =& \varepsilon_{bed}\, A\, dz\, (\rho_b\, c_{p,b} + \sum_i (\rho_{a,i}\, c_{p,a,i}))\, \frac{\partial T_g}{\partial t} \\ &+ \varepsilon_{bed}\, A\, dz\, T_g \sum_i \left(c_{p,a,i}\, \frac{\partial \rho_{a,i}}{\partial t} \right)\end{aligned} \tag{5.23}$$

For the convective transport term the equation 5.24 is assigned. All physical quantities can alter along the column length due to adsorption, temperature- and concentration changes.

$$\frac{\partial \dot{H}_c}{\partial z} = \frac{\partial}{\partial z}\, (\dot{V}\, (\rho_b\, c_{p,b} + \sum_i (\rho_{a,i}\, c_{p,a,i}))\, T_g) \tag{5.24}$$

The diffusive transport term summarises the axial heat conduction within the gas flow as well as the heat conduction within the adsorbent bed.

$$\frac{\partial \dot{H}_d}{\partial z} = \frac{\partial}{\partial z} \left(-\lambda_{ax}\, \varepsilon_{bed}\, A\, \frac{\partial T_g}{\partial z} \right) = -\lambda_{ax}\, \varepsilon_{bed}\, A\, \frac{\partial^2 T_g}{\partial z^2} \tag{5.25}$$

The sensible heat flow and the enthalpy flow of the adsorptive are calculated analogously to chapter 5.3.3.

The heat flow to the wall is defined by a transfer coefficient α_w through the adsorber shell surface $A = 2\,\pi\, r\, dz$ and a temperature gradient between the gas phase temperature T_g and the wall temperature T_w.

$$\dot{Q}_w = \alpha_w\, 2\,\pi\, r\, dz\, (T_g - T_w) \tag{5.26}$$

By inserting the equations 5.16, 5.17 ($\dot{H}_a$-part), 5.23, 5.24, 5.25 and 5.26 into the balance equation 5.19, and considering again the second differential equation 5.10 for all adsorptives, results in the fourth and last differential equation:

$$\begin{aligned}\frac{\partial T_g}{\partial t} =& \frac{1}{\rho_b\, c_{p,b} + \sum_i (\rho_{a,i}\, c_{p,a,i})}\, [\\ & \frac{1}{\epsilon_{bed}\, A}\, [- \frac{\partial (\dot{V}\, (\rho_b\, c_{p,b} + \sum_i (\rho_{a,i}\, c_{p,a,i}))\, T_g)}{\partial z} \\ & + \sum_i \left(\frac{\partial\, (\dot{V}\, \rho_{a,i})}{\partial z}\, c_{p,a,i}\, T_g \right) \\ & + \lambda_{ax}\, \varepsilon_{bed}\, A\, \frac{\partial^2 T_g}{\partial z^2} - \sum_i \left(D_{ax,i}\, \varepsilon_{bed}\, A\, c_{p,a,i}\, T_g\, \frac{\partial^2 \rho_{a,i}}{\partial z^2} \right) \\ & - \alpha_w\, 2\,\pi\, r\, (T_g - T_w)] \\ & + k_h\, A_{ssa}\, \frac{1 - \varepsilon_{bed}}{\varepsilon_{bed}}\, (T_s - T_g)\ ]\end{aligned} \tag{5.27}$$

5.3.5 Gas phase momentum balance

The momentum balance can be set up in an analogous way. For the flow in a bed, the momentum balance can be simplified with the widely applied correlation of Ergun for pressure loss gradient [26, 39, 46, 47].

$$-\frac{\partial p}{\partial z} = 150\, \frac{\eta\, (1 - \varepsilon_{bed})^2}{\varepsilon_{bed}^3\, d_p^2}\, v + 1.75\, \frac{\rho\, (1 - \varepsilon_{bed})^2}{\varepsilon_{bed}^3\, d_p}\, v^2 \tag{5.28}$$

with total pressure p, particle diameter d_p, gas mixture density ρ and dynamic viscosity η, and gas velocity $v = \frac{\dot{V}}{\varepsilon_{bed} A}$.

5.3.6 Initial and boundary conditions

A set of initial and boundary conditions is required in addition to the differential equations described. In the following, the required initial and boundary conditions are defined.

Initial conditions:

The initial conditions result from equilibrium states. At time $t = 0$, thermal equilibrium prevails in the entire adsorber column:

- solid phase: $T_s(z, t = 0) = T_0$
- gas phase: $T_g(z, t = 0) = T_0$

Also, a material equilibrium according to the adsorption isotherms holds for each adsorptive i at time $t = 0$:

- adsorbent loading: $X_i(z, t = 0) = X_{eq,i,0}$
- adsorptive concentration: $\rho_{a,i}(z, t = 0) = \rho_{a,i,0}$

Boundary conditions:
The boundary conditions describe the state of the gas at the inlet to the adsorber:

- total volume flow: $V(z=0,t) = V_{inlet}$
- gas temperature: $T_g(z=0,t) = T_{g,inlet}$
- total pressure: $p_{tot}(z=0,t) = p_{tot,inlet}$
- adsorptive concentration: $\rho_{a,i}(z=0,t) = \rho_{a,i,inlet}$

Also, the column wall temperature along the adsorber is set as:

- column wall temperature: $T_w(z,t) = T_w$

At last, the axial mass and heat dispersion disappear at the outlet of the adsorber.

- material diffusion: $\frac{\partial^2 \rho_{a,i}}{\partial z^2}(z=L,t) = 0$
- heat diffusion: $\frac{\partial^2 T_g}{\partial z^2}(z=L,t) = 0$

5.4 Mass transport

Following the description of transport phenomena in chapter 2.4.1, the adsorptive mass transport k_m is primarily composed of a combined sequential transfer across the boundary layer to the outer surface of the adsorbent particle (stages 1-2), summarised with β, and various pore transport mechanisms (stage 3), summarised with k_p. These two main transport resistances occur sequentially and the overall mass transfer coefficient is defined as

$$k_m = \frac{\beta\, k_p}{\beta + k_p} \tag{5.29}$$

Independent of the adsorbent, the adsorbent particles are described as equivalent spheres. In order to express the geometrical and structural dependency of the transport coefficient, the expressions for pellets from the work of Rezaei and Webley [8] are considered very suitable. For transport coefficient expressions of other geometries and structures such as monoliths, foams or laminates, reference is also made to their work.

5.4.1 Boundary layer mass transport

The transition of the adsorptive molecule from the gas phase to the boundary layer is described as a mass transfer (stage 1), and across this boundary layer to the outer surface of the adsorbent as film diffusion (stage 2). The appropriate dimensionless number characterising these two stages is the Sherwood number Sh. For pellet systems the Wakao and Funazkri correlation [48] is used to calculate k_b:

$$Sh = 2 + 1.1\, Re^{0.6}\, Sc^{0.33} \tag{5.30}$$

The dimensionless numbers of Sherwood, Reynolds and Schmidt are defined as

$$Sh = \frac{\beta\, d_p}{D_m} \tag{5.31}$$

$$Re = \frac{\rho\, v\, d_p}{\eta} \tag{5.32}$$

$$Sc = \frac{\eta}{\rho\, D_m} \tag{5.33}$$

and considering the gas mixture with its density ρ, free velocity v (considering bed fraction ε_{bed}), dynamic viscosity η, molecular diffusivity D_m and diameter of the adsorbent particle d_p as the characteristic length.

The diffusion coefficient $D_{m,i}$ of component within a gas mixture of more than two components is an average of all two-component diffusion coefficients. This can be calculated according to Sutton and Gnoffo or Tavlarides et al. [49, 50], with mole fraction x:

$$D_{m,i} = \frac{1 - x_i}{\sum_{j \neq i} \frac{x_j}{D_{m,ij}}} \tag{5.34}$$

The molecular diffusivity $D_{m,ij}$ within a two-component system is given by the equation of Chapman and Enskog [51, 52]:

$$D_{m,ij} = \frac{1.86 \cdot 10^{-3}\, T_g^{3/2}\, (1/M_a + 1/M_b)^{1/2}}{p\, \sigma_{ab}^2\, \Omega_{ab}} \tag{5.35}$$

in which $D_{m,ij}$ is measured in $\frac{cm^2}{s}$, T_g is the absolute gas temperature, p is the absolute pressure in atmospheres, and M_a and M_b the molar masses of the adsorptive and the bulk gas. Further, the mean collision diameter σ_{ab} and the dimensionless collision integral Ω_{ab} are required. The calculation of these parameters is explained in appendix A.2 based on tabulated data.

The dynamic viscosity η of the gas mixture can be determined through the multi-component expansion of the Chapman-Enskog theory [51]. However, the following semi-empirical formula is preferred which has shown to reproduce measured mixture viscosities within an average deviation of 2% [53]:

$$\eta = \sum_{\alpha=1}^{N} \frac{x_\alpha\, \eta_\alpha}{\sum_\beta x_\beta \Phi_{\alpha\beta}} \tag{5.36}$$

where the dimensionless quantities are

$$\Phi_{\alpha\beta} = \frac{1}{\sqrt{8}} \left(1 + \frac{M_\alpha}{M_\beta}\right)^{-1/2} \left[1 + \left(\frac{\eta_\alpha}{\eta_\beta}\right)^{1/2} \left(\frac{M_\beta}{M_\alpha}\right)^{1/4}\right]^2 \tag{5.37}$$

N is the number of chemical species in the mixture, x_α the mole fraction, η_α the viscosity which generally depends on temperature and pressure and M_α the molecular mass, all respectively from the considered pure species α. Index β refers to all other gas species in the system, excluding considered species α.

The pressure dependence of viscosity is neglected and therefore only calculated in function of temperature using the regression equation of Kleiber and Joh [54, 55], as listed in Appendix A.3 with tabulated data.

5.4.2 Pore mass transport

According to Bathen and Breitbach [16], these four main transport mechanisms take place partly in parallel, partly one after the other. For each mechanism an individual diffusion coefficient is assigned.

- viscous (laminar) flow D_l
- Knudsen diffusion D_k
- free pore (molecular) diffusion D_m
- surface diffusion D_s

The interaction of these mechanisms and thus the interconnection of these diffusion coefficients is summarised with an "effective" diffusion coefficient D_e [8]. In general, this interconnection is largely uncertain in research but there is consensus, that D_k and D_m are the primary transport resistances. With reference to the work of Nikolaidis et al. [56], D_e is defined as

$$D_e = \frac{\varepsilon_p}{\tau} \frac{D_k\, D_m}{D_k + D_m} \tag{5.38}$$

with consideration of the material structure, respectively particle porosity ε_p and tortuosity factor τ for angled pore structures.

To also consider the geometry of the particle [8], the pore transport coefficient k_p is determined from D_e via particle diameter d_p by

$$k_p = \frac{5\, D_e}{d_p/2} \tag{5.39}$$

Below, the determination of all mentioned diffusion coefficients is shown. The free pore diffusion D_m is calculated according to equation 5.35, while for surface diffusion only a value range can be given.

Viscous flow:
Laminar flow occurs when the pore diameter is larger than the free path length of the adsorptive molecules ($d_{pore} > 10\,\lambda_{free}$). D_l is calculated according to Do et al. [34] with the solid phase temperature T_s, the partial pressure and viscosity of the adsorptive p_a resp. η_a as:

$$D_l = \frac{p_a}{R\,T_s} \frac{(d_{pore}/2)^2}{8\,\eta_a} \tag{5.40}$$

Knudsen diffusion:
This takes place exclusively in pores with a diameter significantly smaller than the free path length ($d_{pore} < 0.1\,\lambda_{free}$ or $Kn > 10$). In this case, the collisions between the pore wall and the adsorptive molecules dominate the mass transport. D_k is defined according to He et al. [57] by

$$D_k = \frac{d_{pore}}{3} \sqrt{\frac{8\,R\,T_s}{\pi\,M_a}} \tag{5.41}$$

Surface diffusion:
The adsorbed molecules are transported within the adsorbed phase. D_s is strongly dependent on the binding energy of the respective adsorptive-adsorbent combination. For weakly bound molecules, D_s is within a range of $10^{-7} - 10^{-8}\ \frac{m^2}{s}$, for strong bonds, this value decreases to $10^{-10} - 10^{-11}\ \frac{m^2}{s}$, according to Kast [23]. In this model, a mean value of $D_s = 10^{-9}\ \frac{m^2}{s}$ is used.

5.5 Heat transport

The heat transport in the adsorber takes place, on the one hand between the adsorbent and the gas mixture flowing through, and on the other hand from the gas phase to the column wall.

5.5.1 Solid/gas heat transport

The overall heat transport k_h between solid phase and gas phase is composed of the heat transfer within the boundary layer at the surface of the particle α and the heat conduction within the particle λ_p (stages 5-7 in chapter 2.4.1).

$$k_h = \frac{\alpha\,\lambda_p}{\alpha + \lambda_p} \tag{5.42}$$

The heat transfer coefficient α can basically be calculated according to Gnielinski [58]. Since an analogy can be made to mass transport, the correlation for Nusselt number by Wakao et al. [59] is used. The difference between these two correlations was shown to be minimal.

$$Nu = 2 + 1.1\,Re^{0.6}\,Pr^{0.33} \tag{5.43}$$

The dimensionless numbers of Nusselt, Reynolds and Prandl are defined as

$$Nu = \frac{\alpha\,d_p}{\lambda} \tag{5.44}$$

$$Re = \frac{\rho\,v\,d_p}{\eta} \tag{5.45}$$

$$Pr = \frac{\eta\,c_p}{\lambda} \tag{5.46}$$

and considering again the gas mixture with its density ρ, free velocity v, thermal conductivity λ, heat capacity c_p and diameter of the adsorbent particle d_p as the characteristic length. λ is analogously computed to η in chapter 5.4.1 with reference to appendix A.3 for the calculation of temperature dependent values.

With regard to the total heat transport resistance, the heat conduction within the particle has only a minor significance compared to the heat transfer at the adsorbent surface. The calculation of heat conduction λ_p taking the particle geometry into account is analogously

defined as for pore mass transport, based on adsorbent thermal conductivity λ_s and particle diameter d_p:

$$\lambda_p = \frac{5\,\lambda_s}{d_p/2} \tag{5.47}$$

5.5.2 Gas/wall heat transport

As defined in the modelling, the column wall temperature is set constant. For the heat transfer from the gas, flowing through the fixed bed, to the collumn wall, various correlations can be found in literature [60]. Following correlation was chosen, which was found to be a good fit by Wakao and Kagei [61]:

$$Nu = 0.17\,Re^{0.79} \tag{5.48}$$

5.6 Axial dispersion

For the calculation of axial dispersion in mass and heat transport, correlations from Wakao et al. [4, 48, 59, 61] are applied.

The axial dispersion coefficient D_{ax} is calculated according to the following relation to the molecular diffusion coefficient D_m:

$$\frac{\varepsilon_{bed}\,D_{ax}}{D_m} = 20 + 0.5\,Sc\,Re \tag{5.49}$$

Diffusion in heat transport is based on axial heat conduction λ_{ax}, which is related to thermal conductivity of the gas mixture λ with

$$\frac{\lambda_{ax}}{\lambda} = 7 + 0.5\,Re\,Pr \tag{5.50}$$

6 Results

In this chapter, the simulation results and validation of the developed adsorption model are presented. Finally, the created user software is explained with regard to the current graphical interface and implemented functions.

6.1 Model validation

The developed adsorption model was validated with measurement data from literature. In the following, the reference case is outlined first, followed by the validation of the equilibrium models and simulated column dynamics.

6.1.1 Reference case

The experimental investigations within the work of Siqueira et al. [46] were taken as a comparative case, since comprehensive and detailed informations are provided regarding column geometry, defined boundary conditions, material parameters for adsorbents and adsorptives, measured isotherms and breakthrough curves, both for single and multi-component adsorption.

The data of the adsorption column and the adsorbent are listed in the following table:

Table 6.1: Column and adsorbent data of experiments carried out by Siqueira et al. [46]

Fixed bed column		
bed length	0.54	m
inner diameter	0.028	m
wall thickness	0.0028	m
density wall	7'400	kg/m^3
sp. heat capacity wall	470	J/(kg K)
Adsorbent:		
adsorbent type	aktivated carbon	
mass	0.136	kg
particle diameter	$3 \cdot 10^{-4}$	m
sp. pore volume	$4.6 \cdot 10^{-4}$	m^3/kg
sp. solid volume	$4.2 \cdot 10^{-4}$	m^3/kg
sp. heat capacity	820	J/(kg K)

The column and adsorbent data were taken to calculate those additional parameters required by this model, as described in chapter 2.6, and supplemented with assumptions based on the data for activated carbon in table 2.3.

Table 6.2: Additional bed and adsorbent parameters for simulation

Fixed bed and adsorbent *Simulation input*		
bed density ρ_{bed}	409	kg/m^3
gross density ρ_g	1'136	kg/m^3
net density ρ_n	2'381	kg/m^3
particle diameter d_p	$3 \cdot 10^{-4}$	m
pore diameter d_{pore}	$5 \cdot 10^{-7}$	m
tortuosity factor τ	7	
bed porosity ε_{bed}	0.64	
particle porosity ε_p	0.52	
sp. surface area A_{ssa}	20'000	m^2/m^3
sp. heat capacity $c_{p,s}$	820	J/(kg K)
th. conductivity λ_s	0.75	W/(m K)

The measurements include both isotherms and breakthrough curves. N_2 and CO_2 were measured with He as the inert bulk gas. In addition to the measurements of the single-component breakthrough curves, the multi-component breakthrough curves regarding the ternary mixture N_2/CO_2/He was also measured. Table 6.3 summarises the boundary conditions of the experiments.

Table 6.3: Boundary conditions of breakthrough experiments carried out by Siqeuira et al. [46]

Single-component 1	
gas composition (mole frac.)	90% He/10% CO_2
std. volume flow	6.8 L/min
inlet/wall temperature	298 K
system pressure	6 / 12 / 20 bar
Single-component 2	
gas composition (mole frac.)	90% He/10% N_2
std. volume flow	6.8 L/min
inlet/wall temperature	298 K
system pressure	6 / 12 / 20 bar
Multi-component	
gas composition (mole frac.)	24% He/16% CO_2/60% N_2
std. volume flow	5.4 L/min
inlet/wall temperature	298 K
system pressure	6 bar

6.1.2 Modelled adsorption equilibria

The measured isotherms of the individual adsorption of CO_2 and N_2 at temperatures 298, 323 and 458 K [46] form the basis for the modelling of thermodynamic equilibria. The single isotherm model fits as well as the isosteric method were done by using proper functions from the python package "pyGAPS", developed by Iacomi and Llewellyn [41].

Adsorption isotherms:

The Langmuir model (chapter 2.3.1, equation 2.6) was fitted to the six measured isotherms, resulting in six parameter sets. In order to predict the equilibria for different temperatures during the simulation, the parameters X_{mon} and K_L were supplemented with temperature-dependent functions:

$$X_{mon}(T) = a\,T + b \tag{6.1}$$

$$K_L(T) = K_{L,0}\, e^{\frac{-\Delta h_{ads}}{R\,T}} \tag{6.2}$$

This results in having only one Langmuir equation per adsorptive. Table 6.4 shows the Langmuir model parameters used:

Table 6.4: Langmuir model parameters

Parameter	CO_2	N_2	
a	-0.0009	-0.0002	1/K
b	0.5382	0.1496	–
$K_{L,0}$	$6.2888 \cdot 10^{-5}$	$2.3831 \cdot 10^{-4}$	1/bar
Δh_{ads} (Ø)	-22'800	-15'200	J/mol

In this way, the isotherms can be accurately predicted, as shown in figure 6.1:

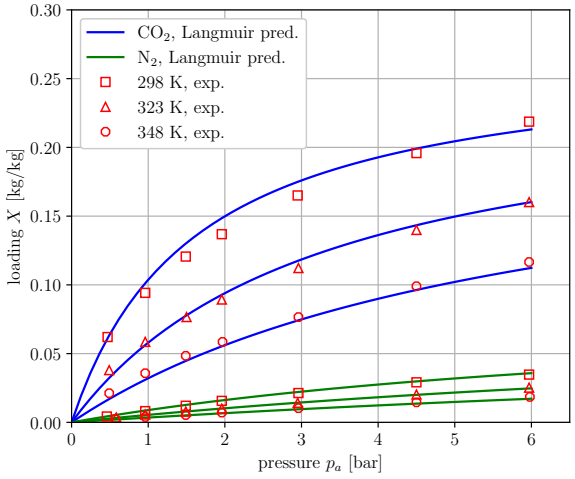

Figure 6.1: Prediction of single-component isotherms at 298, 323, 348 K for CO_2 and N_2

For multi-component isotherms, measurement results are available for a mixture of 15% CO_2 and 85% N_2 [46]. The model parameters of both single isotherms were taken over into the extended Langmuir equation (chapter 2.3.2, equation 2.10). Thus, an appropriate prediction of the mixture equilibrium can also be made, as shown in figure 6.2. Also, it can be seen how the presence of both adsorptives reduces the equilibrium loading of the single isotherms, compared to figure 6.1.

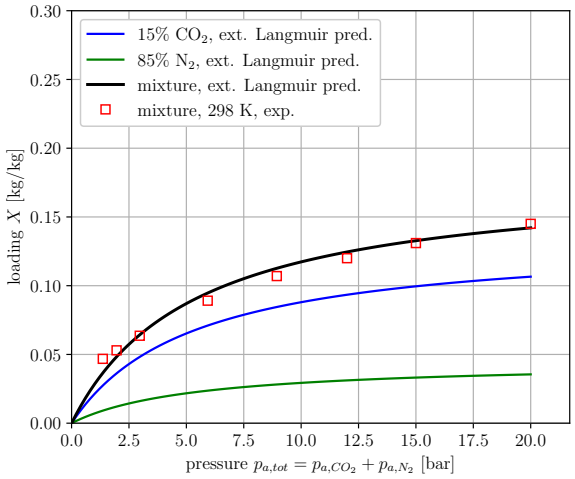

Figure 6.2: Prediction of multi-component isotherms at 298 K for CO_2, N_2 and mixture (15% CO_2, 85% N_2)

Enthalpy of adsorption:

The isosteric method (chapter 2.3.3) was applied to determine the enthalpy of adsorption of the respective adsorptives, based on the three correpsonding isotherms. A polynomial fit was done in order to use the enthalpy as a function of the adsorbent loading in the simulation model.

Figures 6.3 and 6.4 show the determined isosteric enthalpies for CO_2 and N_2 in comparison to the results of Siqueira et al., who applied the same method. While for N_2 the results are practically congruent, for CO_2 clear differences are noticeable. The reason for this may be a differing number of data points generated from the isotherms when applying the isosteric method. However, enthalpy measurement data are not available, which is why the accuracy of the isosteric method in both works can't be validated.

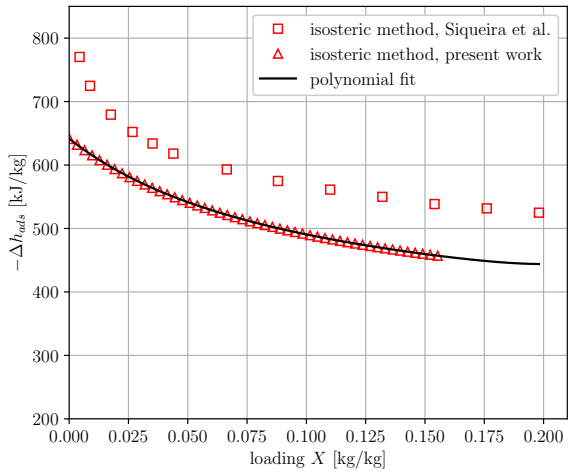

Figure 6.3: Isosteric enthalpy of adsorption for CO_2 as function of adsorbent loading, in comparison to results of Siqueira et al.

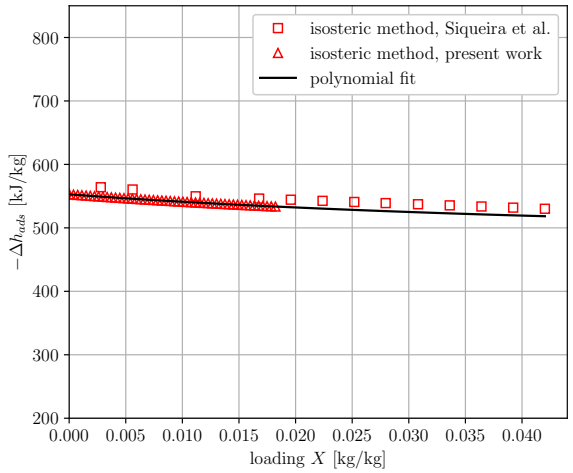

Figure 6.4: Isosteric enthalpy of adsorption for N_2 as function of adsorbent loading, in comparison to results of Siqueira et al.

6.1.3 Simulated column dynamics

In the following, the results of the simulated breakthrough curves are presented. It should be noted that volume flow across the adsorber was set consant and the modelled kinetics was not additionally fitted.

Single-component adsorption:

Figures 6.5 and 6.6 show the simulated and experimental breakthrough curves of single-component adsorption of CO_2 and N_2, each with a mole fraction of 10% in He at 6, 12 and 20 bar and inlet and wall temperature of 298 K.

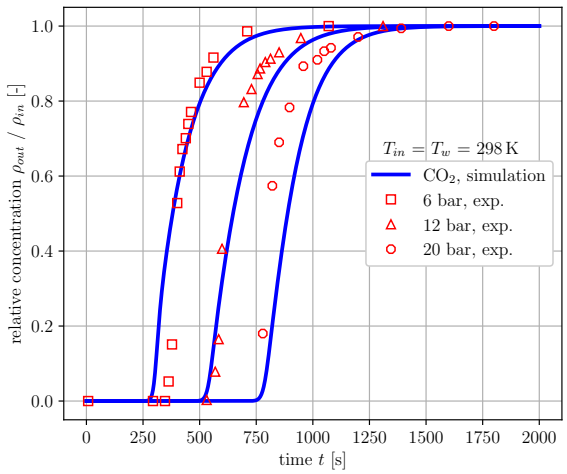

Figure 6.5: Single-component breakthrough curve of CO_2 at 6, 12 and 20 bar and temperature 298 K for inlet and column wall, in comparison to experimental results of Siqueira et al.

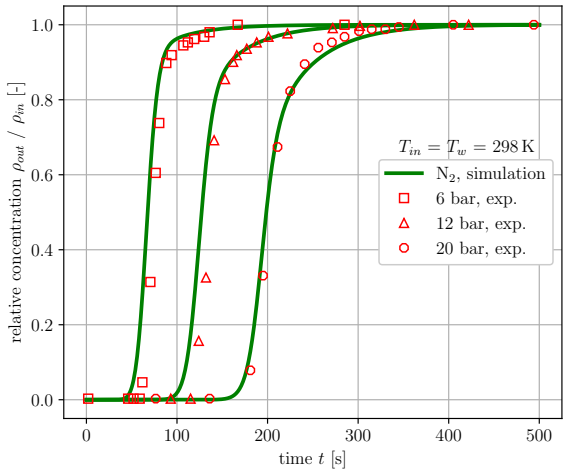

Figure 6.6: Single-component breakthrough curve of N_2 at 6, 12 and 20 bar and temperature 298 K for inlet and column wall, in comparison to experimental results of Siqueira et al.

The breakthrough curves for single-component adsorption can be reproduced with sufficient accuracy. The breakthrough times at 5% relative concentration agree well with the experiments for N_2. However, the breakthrough curve for CO_2 at pressures of 12 and 20 bar, are delayed compared to the experiments.

Multi-component adsorption:

Finally, the simulated and experimental breakthrough curve of multi-component adsorption of CO_2 and N_2 is shown, with mole fractions 16% for CO_2 and 24% for N_2 in He at 6 bar and inlet and wall temperature of 298 K.

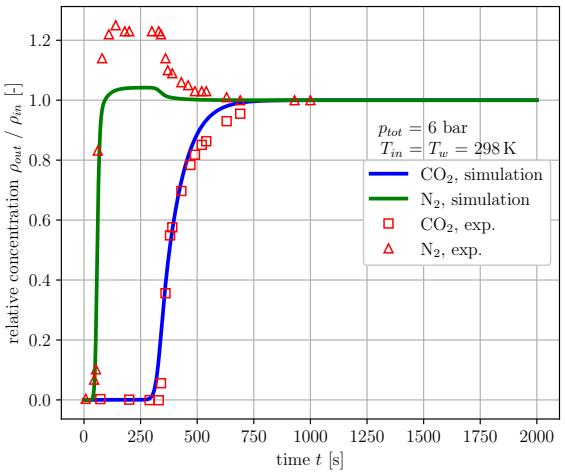

Figure 6.7: Multi-component breakthrough curve of CO_2 and N_2 at 6 bar and temperature 298 K for inlet and column wall, in comparison to experimental results of Siqueira et al.

Qualitatively, the dynamics of multi-component adsorption could be reproduced mostly well. The breakthrough times at 5% relative concentration are in agreement. However, N_2 does not reach the same maximum relative concentration as in the experiments. This is due to a calculation error in the pressure ratios of the gas components, which has not yet been corrected. Also, the bed cools down too fast, which is clearly visible at the curve of CO_2 at around 90% relative concentration.

6.2 User software

The current status of the user software is presented here. It should be noted that many software functions have been realised and are working on their own, but the logical interfaces are not yet functionally embedded in the software. Despite this, the software functions are explained as if they were all embedded in an applicable software.

6.2.1 Input windows

When starting the programme, the user is asked to enter all data for the simulation of the adsorption process. For this purpose, two graphical interfaces were created to enable the input of the parameters and the equilibrium measurement data.

Parameter input

The parameters defined in the software concept are entered in the first window. The parameters are divided into tabs according to defined categories:

- adsorption column data
- adsorbent material properties
- adsorptives material properties
- bulk gas material properties
- process inlet conditions
- initial conditions adsorber
- simulation parameters

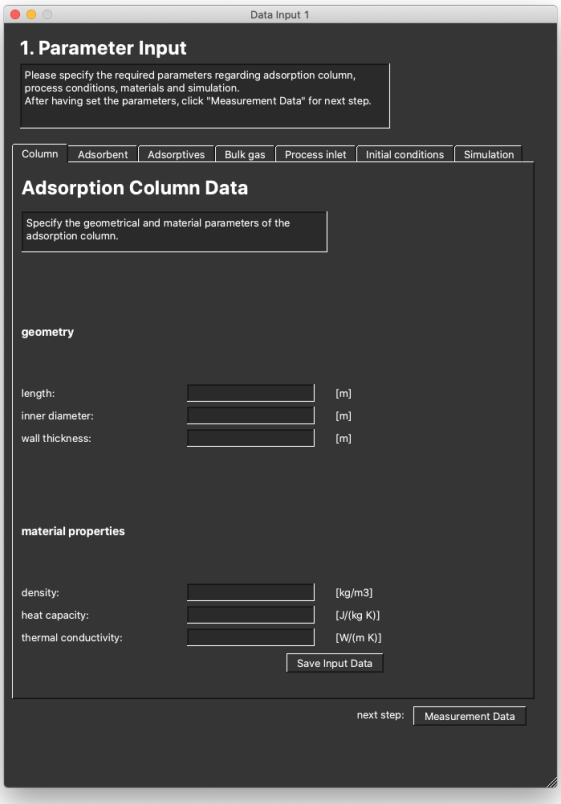

Figure 6.8: Graphical user interface for entering and saving the required parameters (s. Appendix A.4)

The parameter entries are done in the text fields. After this, the user saves the values for each tab by clicking on the button "Save Input Data". An input confirmation appears in the terminal, including further calculated values. Figure 6.9 shows the confirmation of entered column parameters, for example.

```
[>-------------------------------------------<]
[>--- Data Input 1: Adsorption Column Data ------<]
[>-------------------------------------------<]

length:                          0.54 m
inner diameter:                  0.028 m
wall thickness:                  0.0028 m
wall density:                    7400.0 kg/m3
specif. heat capacity (const.): 470.0 J/(kg K)
thermal conductivity (const.):  50.0 W/(m K)

calculated parameters:

outer diameter:                  0.0336 m
bed cross section:               0.00062 m2
column cross section (annulus): 0.00027 m2
bed volume:                      0.00033 m3
column wall volume:              0.00015 m3
column mass:                     1.083 kg
```

Figure 6.9: Terminal confirmation of saved input parameters and further calculated values

After all entries have been made, the button "Measurement Data" is clicked to proceed to the next data entry.

Measurement data input

In the next window, the user is supposed to enter the measured equilibrium data.

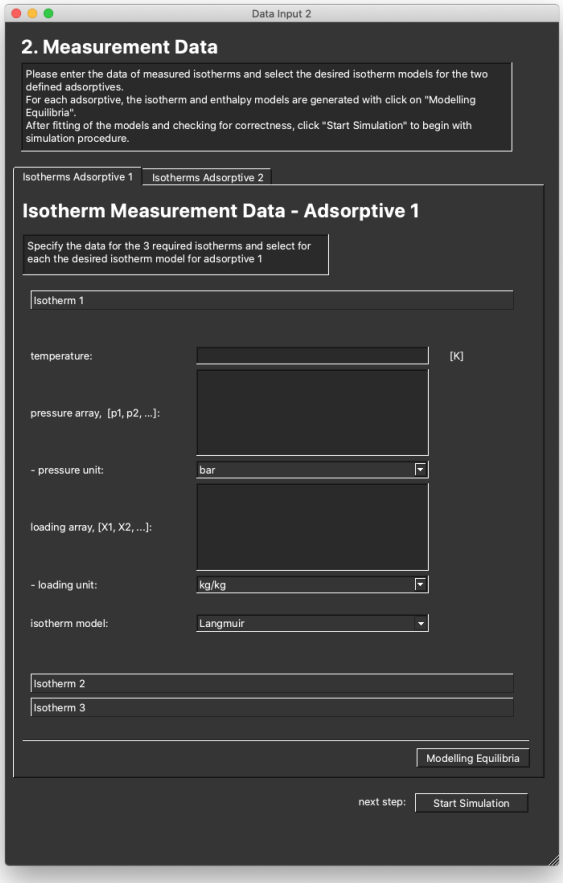

Figure 6.10: Graphical user interface for entering and modelling equilibrium data (s. Appendix A.4)

The software is based on the simulation model for two-component adsorption. This means that data on two adsorptives must be entered in both input windows. It is also defined, that 3 measured isotherms are required for each of the two adsorptives. Two tabs were created for the two adsorptives, with 3 compartments each for entering the measurement data.

In the text fields, the arrays for pressures and loadings can be entered by comma separation. Furthermore, information on the temperature and the units used must be provided so that the data can be processed correctly internally. For example, whether the pressure is in bar or Pa, or whether the loading was measured in kg/kg or mmol/g, among other things. The units can be selected via dropdown widgets.

If data is complete, the equilibrium models for the respective adsorptives can be created by pressing the button "Modelling Equilibria". The software would then generate the defined models for the individual isotherms as well as for the adsorption enthalpy. The user can then check the fits using graphical outputs which appear as pop-up windows. If everything is ok, the button "Start Simulation" can be pressed and the software starts with the simulation algorithm.

6.2.2 Graphical outputs / terminal prints

It is planned that the software will process the input data to create models for isosterms and adsorption enthalpies first, and finally to run the simulation and generate the graphical output windows. A Python module was created for each of these tasks. However, the logical interface between input modules and the modelling respectively simulation module is not yet fully functional.

Modelling of Equilibria

The modelling module reads in the data and fits the defined models to the measurement data. With applied functions from the Python package "pyGAPS" [41], any single isotherms can be modelled basically. However, only the extended Langmuir equation is stored for the multi-component simulation, which is why the applicability of the single isotherm models is severely limited.

The module first summarises the measurement data in the terminal and displays the measurement isotherms graphically, as shown in figures 6.11 and 6.12.

```
Summary of each measured isotherm - info & plot:

Isotherm 1:

Material: activated carbon
Adsorbate: carbon dioxide
Temperature: 298.0K
Units:
        Uptake in: kg/kg
        Pressure in: bar
```

Figure 6.11: Summary of measured isotherm data, excerpt of first isotherm

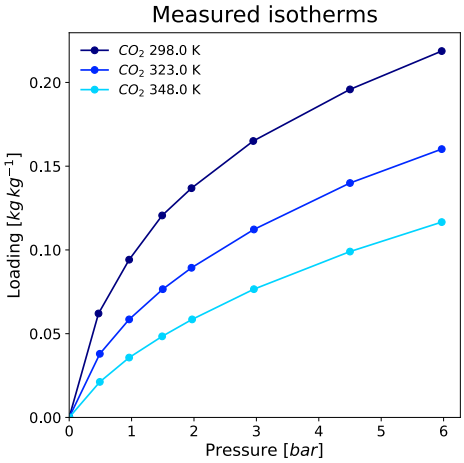

Figure 6.12: Graphical output of measured isotherm data

Afterwards, the models are generated and summarised in analogue form, with detailed information in terminal print, as in figures 6.13 and 6.14. The model isotherms show the generated data points, which are later used when performing the isosteric method.

```
Summary of each isotherm model - info & plot:

Model for isotherm 1:

Attempting to model using Langmuir.
Model Langmuir success, RMSE is 0.004
Material: activated carbon
Adsorbate: carbon dioxide
Temperature: 298.0K
Units:
        Uptake in: kg/kg
        Pressure in: bar
Other properties:
        branch: ads
Langmuir isotherm model.
RMSE = 0.0041
Model parameters:
        K = 0.50
        n_m = 0.29
Model applicable range:
        Pressure range: 0.00 - 5.97
        Loading range: 0.00 - 0.22
```

Figure 6.13: Summary of modelled isotherms, excerpt of first isotherm

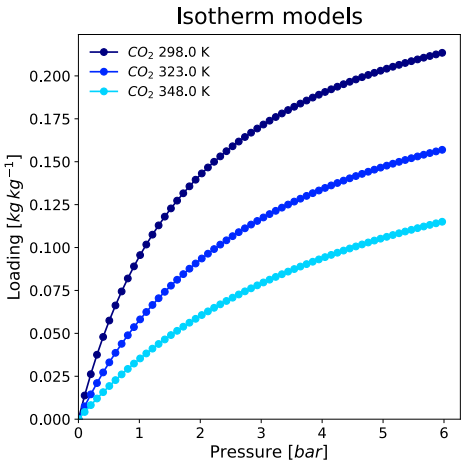

Figure 6.14: Graphical output of modelled isotherms

Finally, the adsorption enthalpy is calculated from the data points of the model isotherms using the isosteric method and is also output graphically.

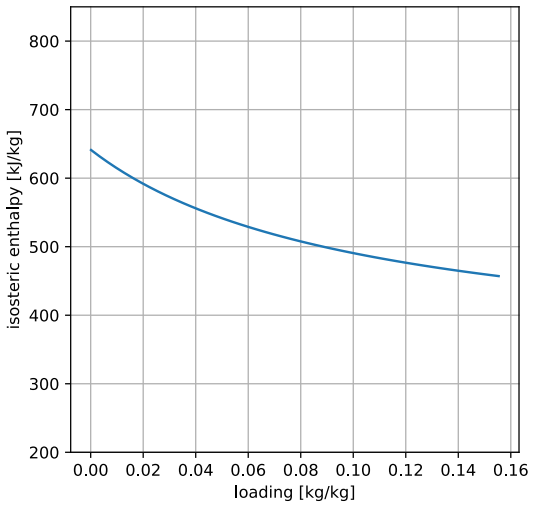

Figure 6.15: Graphical output of enthalpy of adsorption

The model parameters for isotherms and enthalpies are stored in a separate file. Functions for multi-component adsorption were created which read the stored parameters and used in the equilibrium and kinetics module, supporting the simulation module.

Process simulation

The simulation module reads in all input parameters and functions and carries out the simulation. First, a complete overview of all input values and calculated parameters for the adsorber model is displayed in the terminal.

```
[>-------------------------------------------<]
[>--- adsorption column data ----------------<]
[>-------------------------------------------<]

length:                          0.54 m
inner diameter:                  0.028 m
wall thickness:                  0.0028 m
outer diameter:                  0.0336 m
bed cross section:               0.0006 m2
column cross section (annulus): 0.0003 m2
bed volume:                      0.0003 m3
column volume:                   0.0001 m3
wall density:                    7400 kg/m3
column mass:                     1.083 kg
specif. heat capacity (const.): 470 J/(kg K)
thermal conductivity (const.):   50 W/(m K)
[>-------------------------------------------<]
[>--- adsorptives properties (gas phase) -----<]
[>-------------------------------------------<]

adsorptive 1:                    CO2
molar mass:                      0.04401 kg/mol
specif. heat capacity (const.): 875 J/(kg K)
thermal conductivity:            0.017 W/(m K)
dyn. viscosity:                  1.4970203788524134e-05 Pa s
collision diameter:              3.941 Å
interaction potential:           195.2 K

adsorptive 2:                    N2
molar mass:                      0.02801 kg/mol
specif. heat capacity (const.): 1040 J/(kg K)
thermal conductivity:            0.026 W/(m K)
dyn. viscosity:                  1.7750031470436887e-05 Pa s
collision diameter:              3.798 Å
interaction potential:           71.4 K
```

Figure 6.16: Simulation parameters, part 1

```
[>-------------------------------------------<]
[>--- adsorbent properties (solid phase) -----<]
[>-------------------------------------------<]

adsorbent:                       activated carbon
bed density:                     409 kg/m3
adsorbent mass:                  0.136 kg
gross density:                   1136 kg/m3
net density:                     2381 kg/m3
particle diameter                0.0003 m
pore diameter                    5e-07 m
tortuosity factor                7
void fraction / bed porosity:    0.64
particle porosity:               0.52
vol.-specific surface area:      20000 m2/m3
specif. heat capacity (const.): 820 J/(kg K)
thermal conductivity (const.):   0.75 W/(m K)
[>-------------------------------------------<]
[>--- bulk gas properties (gas phase) --------<]
[>-------------------------------------------<]

bulk gas:                        He
molar mass:                      0.00400 kg/mol
specif. heat capacity (const.): 5193 J/(kg K)
thermal conductivity:            0.154 W/(m K)
dyn. viscosity:                  1.981212271159418e-05 Pa s
collision diameter:              2.551 Å
interaction potential:           10.2 K
[>-------------------------------------------<]
[>-- process parameters / boundary conditions -<]
[>-------------------------------------------<]

std. bulk volume flow:           5.400 L/min
bulk volume flow:                0.00002 m3/s
state number:                    0.184
gas velocity through bed:        0.042 m/s

total pressure:                  600000.0 Pa
partial pressure ads. 1:         96000.0 Pa
partial pressure ads. 2:         360000.0 Pa
partial pressure bulk gas:       144000.0 Pa

partial density ads. 1:          1.704 kg/m3
partial density ads. 2:          4.068 kg/m3
partial density bulk gas:        0.233 kg/m3

gas temperature:                 25.0 °C
wall temperature:                25.0 °C
[>-------------------------------------------<]
[>--- initial conditions within adsorber -----<]
[>-------------------------------------------<]

init. bulk volume flow:          0.00002 m3/s
init. gas velocity:              0.042 m/s

init. total pressure:            600000.0 Pa
init. pressure ads. 1:           0.1 Pa
init. pressure ads. 2:           0.1 Pa
init. pressure bulk gas:         599999.9 Pa

init. density ads. 1:            0.000 kg/m3
init. density ads. 2:            0.000 kg/m3
init. density bulk gas:          0.969 kg/m3

init. eq-loading ads. 1:         0.000 kg/kg
init. eq-loading ads. 2:         0.000 kg/kg
init. eq-loading total:          0.000 kg/kg

init. adsorbent temperature      25.0 °C
init. gas temperature            25.0 °C
[>-------------------------------------------<]
[>--- simulation parameters ------------------<]
[>-------------------------------------------<]

simulated time:                  2000 s
time stamps:                     200000
time step:                       0.01 s
number of volume elements:       100
element length:                  0.0054 m
```

Figure 6.17: Simulation parameters, part 2

While the simulation is running, the user receives information about the currently calculated time step. At the end, the simulation time is output. The simulation data are stored, such as the temporally and spatially resolved variables for concentrations, loadings, pressures and temperatures as well as their rates of change.

For the analysis of the simulation results, graphical outputs are generated in which the user can partly interact:

The mass transfer zones and heat curves are output in an interactive window. Specifically, the total and partial loadings of the adsorbent, the relative concentrations as well as the gas and adsorbent temperature are represented with temporal and spatial resolution. The user can set the process time and flexibly adjust the axis sections of the plots.

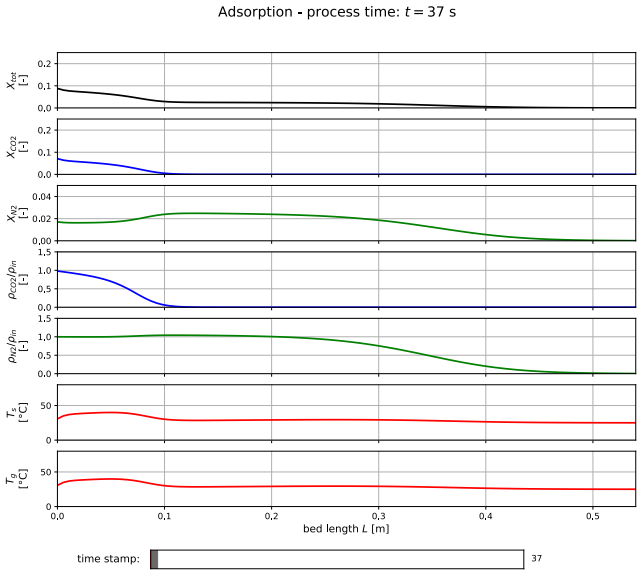

Figure 6.18: Graphical output of mass transfer zones and heat curves, with user interaction on process time (s. Appendix A.5)

The rates of change of the above mentioned variables are also displayed in the same way.

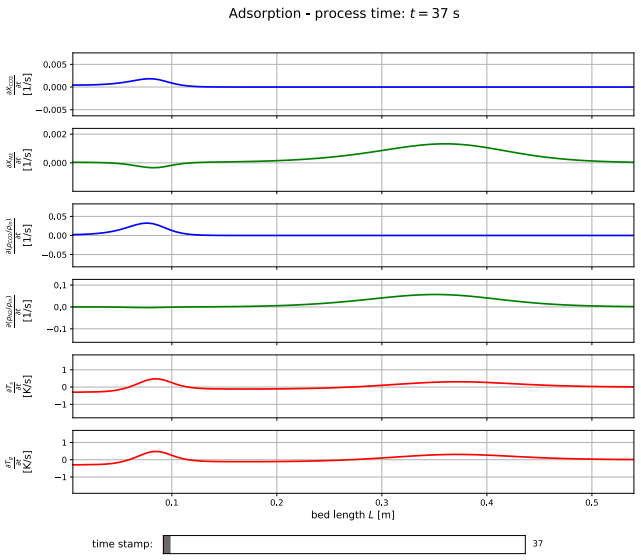

Figure 6.19: Graphical output of the rates of change for loadings, concentrations and temperatures, with user interaction on process time (s. Appendix A.5)

The breakthrough curves are shown for both adsorptives, indicating the concentrations for the characteristic time values breakthrough time (5%), half time (50%) and total time (95%).

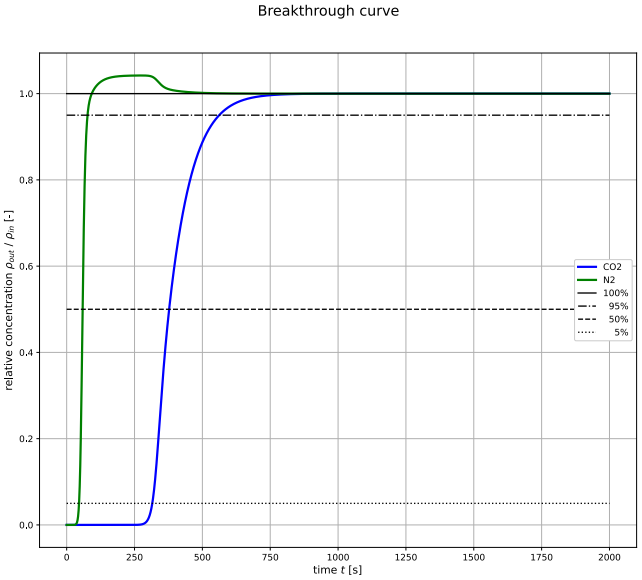

Figure 6.20: Graphical output of the breakthrough curves with characteristic time values (s. Appendix A.5)

Based on the simulation data, further graphical outputs can also be generated, for example the time course of the bed temperature at a certain position or the adsorbed masses.

7 Conclusions

In the final chapter, the content covered is reflected and recommendations for further proceedings are given.

7.1 Discussion

In this work, a mathematical-physical model for multi-component gas phase adsorption has been both developed and validated with measurement data. Additionally, a first version of a user software with graphical interfaces has been created, whose functional framework can be used for modelling equilibria and simulating the process. Everything was implemented in Python.

After defining the requirements for the model and the user software with stakeholders, the basics for modelling of multi-component adsorption and desorption processes were updated with regard to thermodynamics, kinetics and dynamics. Also, research on software development and graphical user interfaces was carried out.

A previously developed simple model was extended to two-component adsorption and validated with measurement data based on a reference case from literature. First, the single-component model was newly developed, validated and corrected, followed by the model extension to the multi-component case and its final validation. Considering that the models did not have to be additionally fitted, the breakthrough curves for one and two components are qualitatively very well reproduced. The breakthrough times are correct and the curves are very similar to the measurements. However, certain inconsistencies exist, for example that in the case of the investigated component N_2 the maximum relative concentrations were not reached, or that for higher system pressures a temporal offset of the breakthrough curves occurs.

For the development of the user software, a concept was first created. Based on a user journey, the contents and the operating sequence of the software were determined and the program structure was defined. Important decisions were that the simulations by the software should be based on measured data and therefore the modeling of the equilibrium models should be as flexible as possible with regard to the isotherm models used. This resulted in the "five design steps", after which the software works. Also the inputs, which are needed by the user, were defined and variants of the graphical user interface were worked out.

During the implementation in Python the primary focus was on the creation of the graphical windows for the input of the parameters and the measurement data of isotherms. Many functions and modules were created, with embedding of the adsorption model for two-components. Regarding the defined requirements, the software functions basically allow the input of all parameters and measurement data, the modelling of the equilibrium models, the execution of the simulation of the adsorption process, as well as the graphical evaluation based on mass transfer zones and breakthrough curves.

While for the validation of the model, all functions and calculations could be designed for a specific reference case, the elaboration of the user software turned out to be very complex, since it must have a great flexibility with respect to different material pairings adsorbent-adsorptive and related equilibrium models. Different single isotherm models can be created, however the program is severely limited when it comes to multi-component models. Even tough the current software has a detailed functional framework, it must be designed more flexible and the interfaces between the individual modules need to be completed.

7.2 Further proceedings

The multi-component adsorption model developed in this project successfully represents the dynamics of fixed-bed adsorbers. Still, there are some inconsistencies as explained in the previous chapters. It is recommended to check the calculations for momentum balance and gas composition with regard to relative concentrations and pressures. Also, the heat transport to the wall must be compared with other correlations. On the other hand, the system boundary of the model could be extended to include pressure, heating and cooling systems for more comprehensive theoretical studies.

The developed user software has a comprehensive functional framework, but the software as a complete entity is not yet fully functional and the flexibility for different measured data and internally calculated material properties is limited. The interfaces between the modules should be completed and also the graphical elements should be integrated into a complete cockpit. With respect to more open equilibrium modelling, more functional classes could be programmed for single- and multi-component isotherms. Concerning the material data, which are required by the thermodynamic and kinetic functions and partly still have to be entered by the user himself, material databases could be stored or the Coolprop Python package could be used to a greater extent.

Currently, the software only allows the simulation of one single adsorption process. With the extension to the subsequent desorption process, it will be possible to calculate technical, energetic and economic key figures as well.

References

[1] K. Sattler, *Thermische Trennverfahren - Grundlagen, Auslegung, Apparate*. WILEY-VCH Verlag GmbH, 2001, ok bro.

[2] A. Kohl and R. Nielsen, *Gas Purification*, 5th ed. Houston: Gulf Publishing Company, 1960.

[3] F. I. Khan and A. Kr. Ghoshal, "Removal of volatile organic compounds from polluted air," *Journal of Loss Prevention in the Process Industries*, vol. 13, no. 6, pp. 527–545, 2000. [Online]. Available: http://www.sciencedirect.com/science/article/pii/S0950423000000073

[4] A. F. P. Ferreira, A. M. Ribeiro, S. Kulaç, and A. E. Rodrigues, "Methane purification by adsorptive processes on MIL-53(Al)," *Chemical Engineering Science*, vol. 124, pp. 79–95, 2015. [Online]. Available: https://www.sciencedirect.com/science/article/pii/S0009250914003017

[5] V. Mulgundmath and F. H. Tezel, "Optimisation of carbon dioxide recovery from flue gas in a TPSA system," *Adsorption*, vol. 16, no. 6, pp. 587–598, 2010. [Online]. Available: https://doi.org/10.1007/s10450-010-9255-9

[6] N. A. A. Qasem and R. Ben-Mansour, "Adsorption breakthrough and cycling stability of carbon dioxide separation from $CO_2/N_2/H_2O$ mixture under ambient conditions using 13X and Mg-MOF-74," *Applied Energy*, vol. 230, pp. 1093–1107, 2018. [Online]. Available: http://www.sciencedirect.com/science/article/pii/S0306261918313783

[7] M. Fischedick, K. Görner, and M. Thomeczek, *CO2: Abtrennung, Speicherung, Nutzung: Ganzheitliche Bewertung im Bereich von Energiewirtschaft und Industrie*. Springer Berlin Heidelberg, 2015. [Online]. Available: https://books.google.ch/books?id=_8K9BwAAQBAJ

[8] F. Rezaei and P. Webley, "Optimum structured adsorbents for gas separation processes," *Chemical Engineering Science*, vol. 64, no. 24, pp. 5182–5191, 2009. [Online]. Available: https://dx.doi.org/10.1016/j.ces.2009.08.029

[9] C. Grande, *Advances in Pressure Swing Adsorption for Gas Separation*, 2012, vol. 2012.

[10] H. Schreiber, S. Graf, F. Lanzerath, and A. Bardow, "Adsorption thermal energy storage for cogeneration in industrial batch processes: Experiment, dynamic modeling and system analysis," *Applied Thermal Engineering*, vol. 89, pp. 485–493, 2015. [Online]. Available: https://www.sciencedirect.com/science/article/pii/S1359431115005694

[11] D. Ursueguía, P. Marín, E. Díaz, and S. Ordóñez, "A new strategy for upgrading ventilation air methane emissions combining adsorption and combustion in a lean-gas turbine," *Journal of Natural Gas Science and Engineering*, vol. 88, p. 103808, 2021. [Online]. Available: https://www.sciencedirect.com/science/article/pii/S1875510021000159

[12] B. El Fil and S. Garimella, "Heat recovery, adsorption thermal storage, and heat pumping to augment gas-fired tumble dryer efficiency," *Journal of Energy Storage*, vol. 48, p. 103949, 2022. [Online]. Available: https://www.sciencedirect.com/science/article/pii/S2352152X21016133

[13] B. Burrichter, "Adsorptive Entfernung von Wasser im unteren ppm-Bereich zur Erzeugung hochreiner organischer Lösungsmittel," Thesis, 2015, ok bro.

[14] D. Bonalumi, S. Lillia, G. Manzolini, and C. Grande, "Innovative process cycle with zeolite (MS13X) for post combustion adsorption," *Energy Procedia*, vol. 114, pp. 2211–2218, 2017. [Online]. Available: http://www.sciencedirect.com/science/article/pii/S1876610217315412

[15] C. Bian, D. Li, Q. Liu, S. Zhang, L. Pang, Z. Luo, Y. Guo, Z. Chen, and T. Li, "Recent progress of Pd/zeolite as passive NO_x adsorber: Adsorption chemistry, structure-performance relationships, challenges and prospects," *Chinese Chemical Letters*, 2021. [Online]. Available: https://www.sciencedirect.com/science/article/pii/S1001841721005660

[16] D. Bathen and M. Breitbach, *Adsorptionstechnik*. Berlin, Heidelberg: Springer-Verlag, 2001.

[17] M. S. Shafeeyan, W. M. A. Wan Daud, and A. Shamiri, "A review of mathematical modeling of fixed-bed columns for carbon dioxide adsorption," *Chemical Engineering Research and Design*, vol. 92, no. 5, pp. 961–988, 2014. [Online]. Available: https://www.sciencedirect.com/science/article/pii/S026387621300347X

[18] R. Blättler, "Modelling and simulation of the dynamics of fixed bed adsorbers," Specialisation Project 2, 2021.

[19] S. Schneider, "Modellierung eines Adsorptionsprozesses aus der Gasphase," Master-Thesis, 2019.

[20] S. Schneider, R. Tamburini, M. Kleingries, and U. C. Müller, "Systematische Konzipierung industrieller Ad- und Desorptionsprozesse (SYSKON) - Schlussbericht," Bundesamt für Energie BFE, Report, 2020.

[21] R. Tamburini, M. Kleingries, and U. C. Müller, "Empfehlungen zum energieeffizienten Einsatz von Adsorptionsprozessen aus der Gasphase," Bundesamt für Energie BFE, Report, 2021.

[22] ——, "Leitfaden zur systematischen Auslegung technischer Adsorptionsprozesse aus der Gasphase," Bundesamt für Energie BFE, Report, 2021.

[23] W. Kast, *Adsorption aus der Gasphase - Ingenieurwissenschaftliche Grundlagen und technische Verfahren*. Weinheim: VCH Verlagsgesellschaft, 1988.

[24] Verein Deutscher Ingenieure, "VDI 3674:2013-04, Abgasreinigung durch Adsorption - Prozessgas- und Abgasreinigung," 2013.

[25] W. J. Thomas and B. Crittenden, *Adsorption Technology and Design*. Oxford: Butterworth-Heinemann, 1998. [Online]. Available: https://www.sciencedirect.com/book/9780750619592/adsorption-technology-and-design

[26] W. Kast, "Adsorption aus der Gasphase — Grundlagen und Verfahren," *Chemie Ingenieur Technik*, vol. 53, no. 3, pp. 160–172, 1981. [Online]. Available: https://onlinelibrary.wiley.com/doi/abs/10.1002/cite.330530304

[27] A. Möller, R. Eschrich, C. Reichenbach, J. Guderian, M. Lange, and J. Möllmer, "Dynamic and equilibrium-based investigations of CO_2-removal from CH_4-rich gas mixtures on microporous adsorbents," *Adsorption*, vol. 23, no. 2, pp. 197–209, 2017. [Online]. Available: https://doi.org/10.1007/s10450-016-9821-x

[28] F. Haraszti, "Mixsorb l: Evaluation and benchmarking," 2020.

[29] I. Langmuir, "The adsorption of gases on plane surfaces of glass, mica and platinum," *Journal of the American Chemical Society*, vol. 40, no. 9, pp. 1361–1403, 1918. [Online]. Available: https://doi.org/10.1021/ja02242a004

[30] U. von Gemmingen, "Anmerkungen zum Henry'schen Bereich adsorptiver Gleichgewichte," *Technische Sorptionsprozesse, VDl-Fortschritt-Berichte, VDl Verlag, Düsseldorf*, vol. 3, no. 554, pp. 53–66, 1998.

[31] ——, "Adsorptive Gasphasengleichgewichte bei kleinem Bedeckungsgrad," *Chemie Ingenieur Technik*, vol. 73, no. 4, pp. 352–357, 2001. [Online]. Available: https://onlinelibrary.wiley.com/doi/abs/10.1002/1522-2640%28200104%2973%3A4%3C352%3A%3AAID-CITE352%3E3.0.CO%3B2-N

[32] H. Freundlich, "Über die Adsorption in Lösungen," *Zeitung der Physikalischen Chemie*, vol. 57, pp. 385–470, 1908.

[33] R. Sips, "On the structure of a catalyst surface," *The Journal of Chemical Physics*, vol. 16, no. 5, pp. 490–495, 1948. [Online]. Available: https://aip.scitation.org/doi/abs/10.1063/1.1746922

[34] D. D. Do, *Adsorption analysis : equilibria and kinetics*. London: Imperial College Press, 1998. [Online]. Available: http://site.ebrary.com/id/10734777

[35] National Institute of Standards and Technology, "NIST/ARPA-E database of novel and emerging adsorbent materials (nist isodb)." [Online]. Available: https://adsorption.nist.gov/isodb/index.php#home

[36] A. L. Myers and J. M. Prausnitz, "Thermodynamics of mixed-gas adsorption," *AIChE Journal*, vol. 11, no. 1, pp. 121–127, 1965. [Online]. Available: https://aiche.onlinelibrary.wiley.com/doi/abs/10.1002/aic.690110125

[37] W. Rudzinski, W. A. Steele, and G. Zgrablich, *Equilibria and Dynamics of Gas Adsorption on Heterogeneous Solid Surfaces*, ser. Studies in Surface Science and Catalysis. Elsevier, 1997, vol. 104.

[38] A. Hauer, "Beurteilung fester Adsorbentien in offenen Sorptionssystemen für energetische Anwendungen," Dissertation, 2002.

[39] D. M. Ruthven, *Principles of Adsorption and Adsorption Processes*. New York: John Wiley and Sons, 1984.

[40] A. Nuhnen and C. Janiak, "A practical guide to calculate the isosteric heat/enthalpy of adsorption via adsorption isotherms in metal–organic frameworks, mofs," *Dalton Transactions*, vol. 49, no. 30, pp. 10 295–10 307, 2020. [Online]. Available: http://dx.doi.org/10.1039/D0DT01784A

[41] P. Iacomi and P. L. Llewellyn, "pyGAPS: a Python-based framework for adsorption isotherm processing and material characterisation," *Adsorption*, vol. 25, no. 8, pp. 1533–1542, 2019. [Online]. Available: https://dx.doi.org/10.1007/s10450-019-00168-5

[42] R. Blättler, M. Y. Reich, A. Rettig, T. Sergi Yanez, S. Tresch, R. Waser, D. Widmer, U. C. Müller, and M. Kleingries, "Systematische Konzipierung industrieller Ad- und Desorptionsprozesse (SYSKON) - AP1 State of the Art," Bundesamt für Energie BFE, Report, 2018.

[43] D. Bathen and F. Berg, "Dynamic simulation of gas-phase adsorption processes," *Symposium on Dynamic Sorption*, 2018.

[44] Q. G. . C. KG, "Breakthrough curves," 2021. [Online]. Available: https://www.dynamicsorption.com/dynamic-sorption-method/breakthrough-measurement/

[45] R. T. Yang, *Gas Separation by Adsorption Processes*. Butterworth-Heinemann, 1987. [Online]. Available: https://www.sciencedirect.com/science/article/pii/B9780409900040500015

[46] R. M. Siqueira, G. R. Freitas, H. R. Peixoto, J. F. d. Nascimento, A. P. S. Musse, A. E. B. Torres, D. C. S. Azevedo, and M. Bastos-Neto, "Carbon dioxide capture by pressure swing adsorption," *Energy Procedia*, vol. 114, pp. 2182–2192, 2017. [Online]. Available: http://www.sciencedirect.com/science/article/pii/S1876610217315382

[47] T. Dantas, F. Luna, I. Jr, A. Torres, D. Azevedo, A. Rodrigues, and R. Moreira, "Modeling of the fixed-bed adsorption of carbon dioxide and a carbon dioxidenitrogen mixture on zeolite 13X," *Brazilian Journal of Chemical Engineering*, vol. 28, pp. 533–54 448, 2011.

[48] N. Wakao and T. Funazkri, "Effect of fluid dispersion coefficients on particle-to-fluid mass transfer coefficients in packed beds: Correlation of Sherwood numbers," *Chemical Engineering Science*, vol. 33, no. 10, pp. 1375–1384, 1978. [Online]. Available: https://www.sciencedirect.com/science/article/pii/0009250978851203

[49] K. Sutton and P. Gnoffo, "Multi-component diffusion with application to computational aerothermodynamics," 1998. [Online]. Available: https://arc.aiaa.org/doi/abs/10.2514/6.1998-2575

[50] L. Tavlarides, S. Yiacoumi, C. Tsouris, J. Gabitto, and D. DePaoli, "Sorption modeling and verification for off-gas treatment," Report, 2016-12-20 2016. [Online]. Available: https://www.osti.gov/biblio/1339639https://www.osti.gov/servlets/purl/1339639

[51] J. O. Hirschfelder, C. F. Curtiss, and R. B. Bird, *The Molecular Theory of Gases and Liquids*. John Wiley and Sons, 1964.

[52] E. L. Cussler, *Diffusion Mass Transfer in Fluid Systems.*, 3rd ed. Cambridge University Press, 2009.

[53] R. B. Bird, W. E. Stewart, and E. N. Lightfoot, *Transport Phenomena*, 2nd ed. John Wiley and Sons, 2002.

[54] M. Kleiber and R. Joh, *Berechnungsmethoden für Stoffeigenschaften*. Berlin, Heidelberg: Springer Berlin Heidelberg, 2006, pp. 103–132. [Online]. Available: https://doi.org/10.1007/978-3-540-32218-4_10

[55] ——, *Stoffwerte von sonstigen chemisch einheitlichen Flüssigkeiten und Gasen*. Berlin, Heidelberg: Springer Berlin Heidelberg, 2006, pp. 249–294. [Online]. Available: https://doi.org/10.1007/978-3-540-32218-4_18

[56] G. Nikolaidis, E. Kikkinides, and M. Georgiadis, "A model-based approach for the evaluation of materials and processes for post-combustion carbon dioxide capture from flue gas by PSA/VSA processes," *Industrial and Engineering Chemistry Research*, vol. 55, 2016.

[57] W. He, W. Lv, and J. H. Dickerson, *Gas Transport in Solid Oxide Fuel Cells*. Cham: Springer International Publishing, 2014. [Online]. Available: https://doi.org/10.1007/978-3-319-09737-4_1

[58] V. Gnielinski, *G9 Wärmeübertragung Partikel – Fluid in durchströmten Haufwerken*. Berlin, Heidelberg: Springer Berlin Heidelberg, 2013, pp. 839–840. [Online]. Available: https://doi.org/10.1007/978-3-642-19981-3_50

[59] N. Wakao, S. Kaguei, and T. Funazkri, "Effect of fluid dispersion coefficients on particle-to-fluid heat transfer coefficients in packed beds: Correlation of Nusselt numbers," *Chemical Engineering Science*, vol. 34, no. 3, pp. 325–336, 1979. [Online]. Available: https://www.sciencedirect.com/science/article/pii/0009250979850642

[60] C.-H. Li and B. A. Finlayson, "Heat transfer in packed beds—a reevaluation," *Chemical Engineering Science*, vol. 32, no. 9, pp. 1055–1066, 1977. [Online]. Available: https://www.sciencedirect.com/science/article/pii/0009250977801437

[61] N. Wakao and S. Kagei, *Heat and mass transfer in packed beds*. New York: Gordon and Breach Science Publishers, 1982.

A Appendix

A.1 Definition of terms

In order to have a common understanding of the adsorption concept, the key terms used in this work are defined as follows:

Adsorption: Accumulation of a molecule from a gaseous (or liquid) phase to the surface of a solid material. These surfaces are in particular the inner surfaces of porous solids. This is an exothermic process.

Desorption: Removal of an adsorbed molecule from a solid and transfer to the free fluid phase which is an endothermic process (reversal of adsorption).

Adsorbent: Solid material which binds the molecule to be adsorbed.

Adsorptive: The molecule to be adsorbed which is in the fluid phase (non-adsorbed molecule).

Adsorpt: Molecule which is bound to the adsorbent (adsorbed molecule).

Adsorbate: Two-component system of the asdsorbed adsorptive molecules and the solid adsorbent.

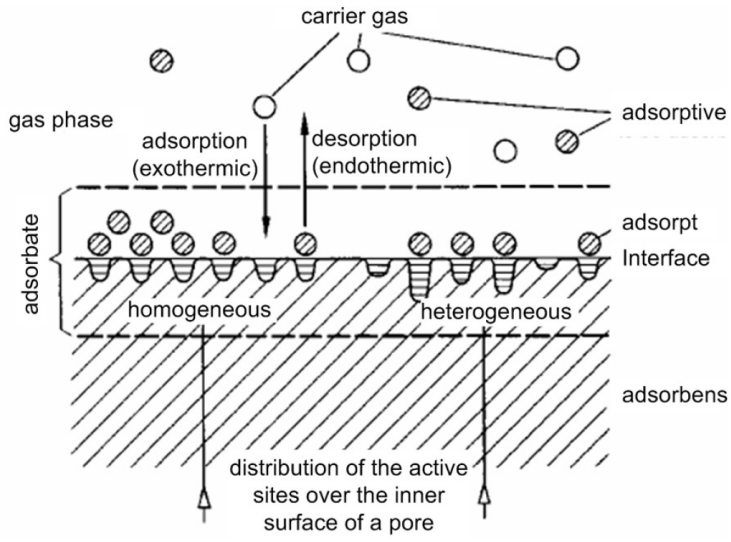

Figure A.1: Basic concept of adsorption [24]

A.2 Molecular diffusion: mean collision diameter and collision integral

In order calculate the molecular diffusion equation 5.35, the values of mean collision diameter σ_{12} and collision integral Ω are needed. The following procedure is to be applied [51, 52]: Values for the collision diameters σ_1 and σ_2 can be found in table A.1. σ_{12} is calculated by

$$\sigma_{12} = \frac{\sigma_1 + \sigma_2}{2} \tag{A.1}$$

The calculation of the collision integral Ω_{12} is based on an interaction between the two gas components. This interaction is described by the Lennard-Jones potential ε_i/k_B:

$$\varepsilon_{12} = \sqrt{\varepsilon_1 \, \varepsilon_2} \tag{A.2}$$

The values for ε_i can be taken from the table A.1. With ε_{12} calculated, Ω_{12} can be found as a function of $\frac{\varepsilon_{12}}{k_B T}$ using the table A.2.

Table A.1: Collision diameter σ and Lennard-Jones potential ε_i/k_B of some gases [51, 52]

Substance		σ(Å)	ε_{12}/k_B(K)
Ar	Argon	3.542	93.3
He	Helium	2.551	10.2
Kr	Krypton	3.655	178.9
Ne	Neon	2.820	32.8
Xe	Xenon	4.047	231.0
Air	Air	3.711	78.6
Br_2	Bromine	4.296	507.9
CCl_4	Carbon tetrachloride	5.947	322.7
$CHCl_3$	Chloroform	5.389	340.2
CH_2Cl_2	Methylene chloride	4.898	356.3
CH_3Cl	Methyl chloride	4.182	350.0
CH_3OH	Methanol	3.626	481.8
CH_4	Methane	3.758	148.6
CO	Carbon monoxide	3.690	91.7
CO_2	Carbon dioxide	3.941	195.2
CS_2	Carbon disulfide	4.483	467.0
C_2H_2	Acetylene	4.033	231.8
C_2H_4	Ethylene	4.163	224.7
C_2H_6	Ethane	4.443	215.7
C_2H_5Cl	Ethyl chloride	4.898	300.0
C_2H_5OH	Ethanol	4.530	362.6
CH_3OCH_3	Methyl ether	4.307	395.0
CH_2CHCH_3	Propylene	4.678	298.9
C_3H_8	Propane	5.118	237.1
n-C_3H_7OH	n-Propyl alcohol	4.549	576.7
CH_3COCH_3	Acetone	4.600	560.2
n-C_4H_{10}	n-Butane	4.687	531.4
iso-C_4H_{10}	Isobutane	5.278	330.1
n-C_5H_{12}	n-Pentane	5.784	341.1
C_6H_6	Benzene	5.349	412.3
C_6H_{12}	Cyclohexane	6.182	297.1
n-C_6H_{14}	n-Hexane	5.949	399.3
Cl_2	Chlorine	4.217	316.0
HBr	Hydrogen bromide	3.353	449.0
HCN	Hydrogen cyanide	3.630	569.1
HCl	Hydrogen chloride	3.339	344.7
HF	Hydrogen fluoride	3.148	330.0
HI	Hydrogen iodide	4.211	288.7
H_2	Hydrogen	2.827	59.7
H_2O	Water	2.641	809.1
H_2S	Hydrogen sulfide	3.623	301.1
Hg	Mercury	2.969	750.0
NH_3	Ammonia	2.900	558.3
NO	Nitric oxide	3.492	116.7
N_2	Nitrogen	3.798	71.4
N_2O	Nitrous oxide	3.828	232.4
O_2	Oxygen	3.467	106.7
SO_2	Sulfur dioxide	4.112	335.4

Table A.2: Dependence of the collision integral Ω on k_B/ε_{12} [51, 52]

k_BT/ε_{12}	Ω	k_BT/ε_{12}	Ω	k_BT/ε_{12}	Ω
0.30	2.662	1.65	1.153	4.0	0.8836
0.40	2.318	1.75	1.128	4.2	0.8740
0.50	2.066	1.85	1.105	4.4	0.8652
0.60	1.877	1.95	1.084	4.6	0.8568
0.70	1.729	2.1	1.057	4.8	0.8492
0.80	1.612	2.3	1.026	5.0	0.8422
0.90	1.517	2.5	0.9996	7	0.7896
1.00	1.439	2.7	0.9770	9	0.7556
1.10	1.375	2.9	0.9576	20	0.6640
1.30	1.273	3.3	0.9256	60	0.5596
1.50	1.198	3.7	0.8998	100	0.5130
1.60	1.167	3.9	0.8888	300	0.4360

A.3 Dynamic viscosity and thermal conductivity of gases

According to Kleiber and Jah [54, 55], the dynamic viscosity and thermal conductivity of species i can be calculated with the following regression equations A.3 resp. A.4 in function of absolute temperature, based on experimental data of the authors. Required parameters can be taken from tables A.3 resp. A.4.

Dynamic viscosity:

$$\eta_i = A_i + B_i \cdot T + C_i \cdot T^2 + D_i \cdot T^3 + E_i \cdot T^4 \tag{A.3}$$

Table A.3: Dynamic viscosity of gases i at low pressures in μ Pa s [55]

Stoff	Formel	Temperatur [°C]								Gl. 3				
		–50	0	25	100	200	300	400	500	10^5 A	10^7 B	10^{10} C	10^{12} D	10^{15} E
Elemente														
Xenon	Xe	17,4	21,3	23,2	28,6	35,3	41,5	47,3	52,7	–0,23692	0,98454	–0,48314	0,01953	–0,00342
Krypton	Kr	19,6	23,5	25,4	30,8	37,5	43,5	49,1	54,2	–0,07920	1,02624	–0,55428	0,02187	–0,00369
Argon	Ar		21,1	22,6	27,0	32,5	37,5	42,2	46,5	0,16196	0,81279	–0,41263	0,01668	–0,00276
Neon	Ne	25,4	29,6	31,5	37,1	43,7	49,6	54,9	59,9	0,23014	1,22527	–0,97141	0,05386	–0,01103
Helium	He	16,2	18,6	19,8	23,2	27,4	31,3	35,1	38,6	0,39223	0,61300	–0,31007	0,01479	–0,00284
Luft		14,6	17,2	18,5	21,9	26,1	29,8	33,2	36,5	–0,01702	0,79965	–0,72183	0,04960	–0,01388
Wasserstoff	H_2	7,3	8,3	8,9	10,4	12,2	14,0	15,6	17,1	0,18024	0,27174	–0,13395	0,00585	–0,00104
Stickstoff	N_2	14,0	16,5	17,8	21,1	25,2	28,7	32,0	35,0	–0,01020	0,74785	–0,59037	0,03230	–0,00673
Sauerstoff	O_2	16,2	19,2	20,7	24,7	29,5	33,8	37,7	41,4	–0,10257	0,92625	–0,80657	0,05113	–0,01295
Schwefel	S					6,9	8,3	9,7	11,1	0,09670	0,11835	0,01588		
Fluor	F_2	18,1	21,5	23,2	27,8	33,6	38,9	43,9	48,7	–0,11373	1,03844	–0,96327	0,08073	–0,02846
Chlor	Cl_2	10,0	12,3	13,4	16,6	20,8	24,8	28,6	32,2	–0,06348	0,49801	–0,09451		
Brom	Br_2		14,3	15,4	19,0	23,8	28,7			0,19483	0,43743	0,05031		
Iod	I_2					21,8	26,0	30,2	34,3	0,06758	0,46358	–0,03714		
Anorganische Verbindungen														
Fluorwasserstoff	HF			11,3	16,0					–7,08883	4,18933	–1,19859	–1,98523	2,59754
Chlorwasserstoff	HCl	10,8	13,4	14,6	18,3	22,9	27,3	31,5	35,4	–0,12146	0,56696	–0,12126		
Bromwasserstoff	HBr	13,8	16,6	18,1	22,2	27,7	33,1	38,5	43,7	0,09163	0,58825	–0,04531		
Iodwasserstoff	HI		17,4	19,0	23,5	29,4	35,1			–0,01823	0,67176	–0,09695		
Cyanwasserstoff	HCN				3,6					–0,06954	0,08177	0,09107		
Wasser	H_2O		9,1	9,9	12,4	16,2	20,3	24,5	28,6	0,64966	–0,15102	1,15935	–0,10080	0,03100
Schwefelwasserstoff	H_2S		11,7	12,6	15,7	20,6				0,54442	0,10851	0,44565		
Ammoniak	NH_3	7,4	9,2	10,1	12,9	16,5	20,1	23,7	27,4	–0,07883	0,36749	–0,00451		
Stickstoffmonoxid	NO	14,9	17,8	19,1	22,9	27,3	31,2	34,8	38,0	–0,09105	0,84998	–0,71473	0,04240	–0,01020
Stickstoffdioxid	NO_2				18,7	24,6	29,4	33,6	37,4	–2,28505	1,75834	–2,29768	0,17134	–0,04920
Distickstoffmonoxid	N_2O	11,0	13,4	14,6	18,1	22,4	26,4	30,0	33,4	–0,09569	0,57181	–0,16548		
Distickstofftetroxid	N_2O_4	13,5	16,6	18,1	22,5	28,2	33,6	38,7	43,6	–0,08683	0,67450	–0,12834		
Dicyan	C_2N_2		9,3	10,1	12,7	16,0	19,3			–0,00521	0,34573	–0,01265		
Phosphortrichlorid	PCl_3	7,8	9,6	10,5	13,2	16,6	19,8	22,9	26,0	–0,11382	0,42969	–0,14926	0,00744	–0,00177
Cyanchlorid	ClCN	6,2	7,6	8,4	10,4	13,1	15,6	18,0	20,2	–0,07162	0,32567	–0,07104		
Silan	SiH_4	8,9	10,7	11,6	14,2	17,8	21,3	24,8	28,4	0,10189	0,35395			
Tetrachlorsilan	$SiCl_4$	7,5	9,3	10,2	12,8	16,1	19,2	22,2	25,1	–0,13422	0,42941	–0,15995	0,00734	–0,00161
Kohlenmonoxid	CO	14,0	16,5	17,7	20,9	24,9	28,4	31,5	34,5	0,01384	0,74306	–0,62996	0,03948	–0,01032
Kohlendioxid	CO_2	11,2	13,8	15,0	18,4	22,6	26,5	30,0	33,3	–0,18024	0,65989	–0,37108	0,01586	–0,00300
Kohlensuboxid	C_3O_2	9,1	11,2	12,2	15,2	19,0	22,6	26,1	29,4	–0,05865	0,45539	–0,08739		
Kohlenoxisulfid	COS	9,5	11,7	12,8	16,0	20,2	24,1	27,8	31,4	–0,10565	0,49410	–0,09608		
Phosgen	CCl_2O			9,3	11,6	14,6	17,3	20,0	22,5	–0,06483	0,35637	–0,07409		
Schwefelkohlenstoff	CS_2	7,3	9,0	9,9	12,5	16,0	19,4	22,7	26,0	–0,07840	0,36608	–0,02490		
Schwefeldioxid	SO_2	9,5	11,8	12,9	16,1	20,3	24,2	27,9	31,3	–0,13559	0,51230	–0,11626		
Schwefeltrioxid	SO_3			13,6	16,8	20,9	24,7	28,1		–0,12683	0,54605	–0,16261		
Sulfurylchlorid	Cl_2SO_2	8,1	10,1	11,1	14,1	17,9	21,6	25,2	28,6	–0,12421	0,43363	–0,06167		
Schwefelhexafluorid	SF_6	10,8	13,6	15,0	18,7	23,2	27,3	30,9	34,3	–0,41132	0,77468	–0,51939	0,02409	–0,00438

Thermal conductivity:

$$\lambda_i = A_i + B_i \cdot T + C_i \cdot T^2 + D_i \cdot T^3 + E_i \cdot T^4 \tag{A.4}$$

Table A.4: Thermal conductivity of gases i at low pressures in W/(m K) [55]

Stoff	Formel	Temperatur [°C]								Gl. 5				
		–50	0	25	100	200	300	400	500	10^3 A	10^3 B	10^6 C	10^9 D	10^{12} E
Elemente														
Xenon	Xe	0,0043	0,0052	0,0056	0,0069	0,0086	0,0102	0,0117	0,0132	–0,006	0,01991	–0,003680		
Krypton	Kr	0,0073	0,0088	0,0095	0,0115	0,0140	0,0163	0,0184	0,0204	–0,389	0,03873	–0,021190	0,008780	–0,001520
Argon	Ar		0,0166	0,0177	0,0209	0,0249	0,0288	0,0326	0,0362	4,303	0,04728	–0,007780		
Neon	Ne	0,0393	0,0459	0,0490	0,0578	0,0682	0,0774	0,0858	0,0936	2,778	0,19430	–0,155500	0,086380	–0,017700
Helium	He	0,1263	0,1446	0,1536	0,1793	0,2116	0,2420	0,2708	0,2983	34,000	0,45661	–0,214890	0,100710	–0,019140
Luft		0,0204	0,0244	0,0263	0,0317	0,0383	0,0444	0,0502	0,0557	–0,908	0,11161	–0,084333	0,056964	–0,015631
Wasserstoff	H_2	0,1429	0,1685	0,1807	0,2149	0,2566	0,2952	0,3319	0,3678	0,651	0,76730	–0,687050	0,506510	–0,138540
Stickstoff	N_2	0,0198	0,0237	0,0256	0,0309	0,0375	0,0437	0,0495	0,0551	–0,133	0,10149	–0,060650	0,033610	–0,007100
Sauerstoff	O_2	0,0201	0,0244	0,0264	0,0324	0,0398	0,0468	0,0534	0,0597	–1,285	0,10655	–0,052630	0,025680	–0,005040
Schwefel	S								0,0145	1,596	0,01559	0,001450		
Fluor	F_2	0,0195	0,0237	0,0258	0,0318	0,0395	0,0469	0,0539	0,0605	–0,246	0,09283	–0,018470		
Chlor	Cl_2	0,0063	0,0081	0,0089	0,0115	0,0147	0,0179	0,0210	0,0239	–1,867	0,03800	–0,006090		
Brom	Br_2				0,0061	0,0089				5,455	–0,01846	0,054230		
Iod	I_2					0,0052	0,0063	0,0074	0,0085	–0,014	0,01097	0,000020		
Anorganische Verbindungen														
Fluorwasserstoff	HF	0,0167	0,0198	0,0214	0,0263	0,0329	0,0396	0,0464	0,0534	2,921	0,05998	0,006940		
Chlorwasserstoff	HCl	0,0112	0,0134	0,0146	0,0179	0,0224	0,0269	0,0314	0,0359	1,233	0,04459	0,000370		
Bromwasserstoff	HBr	0,0061	0,0077	0,0086	0,0110	0,0142	0,0173			–1,740	0,03605	–0,004870		
Iodwasserstoff	HI		0,0056	0,0061	0,0077	0,0098	0,0118	0,0138	0,0157	–0,308	0,02216	–0,001840		
Cyanwasserstoff	HCN		0,0098	0,0118	0,0178	0,0259	0,0338	0,0418		–12,121	0,08049	–0,000500		
Wasser	H_2O			0,0185	0,0239	0,0329	0,0433	0,0547	0,0669	13,918	–0,04699	0,258066	–0,183149	0,055092
Schwefelwasserstoff	H_2S	0,0083	0,0126	0,0144	0,0190	0,0247	0,0308			–37,786	0,36576	–0,980220	1,341110	–0,662840
Ammoniak	NH_3		0,0221	0,0251	0,0344	0,0476	0,0618	0,0770	0,0931	–6,678	0,09224	0,047670		
Stickstoffmonoxid	NO	0,0196	0,0236	0,0255	0,0312	0,0383	0,0449	0,0509		0,144	0,09295	–0,02601		
Stickstoffdioxid	NO_2				0,0280					66,085	–0,47937	1,011240		
Distickstoffmonoxid	N_2O	0,0119	0,0157	0,0176	0,0234	0,0310	0,0388	0,0465	0,0543	–5,049	0,07561	0,001460		
Distickstofftetroxid	N_2O_4				0,0280					66,085	–0,47937	1,011240		
Dicyan	C_2N_2		0,0144	0,0160	0,0211	0,0280	0,0351	0,0424	0,0499	–2,939	0,06067	0,009930		
Phosphortrichlorid	PCl_3	0,0053	0,0068	0,0075	0,0098	0,0127	0,0156	0,0183	0,0209	–1,274	0,02818	0,008226	–0,013677	0,005121
Cyanchlorid	ClCN			0,0094	0,0122	0,0160	0,0196	0,0231	0,0265	–2,531	0,04158	–0,005290		
Silan	SiH_4	0,0157	0,0204	0,0228	0,0305	0,0416	0,0534	0,0659	0,0788	–1,601	0,06205	0,074888	–0,029302	0,003487
Tetrachlorsilan	$SiCl_4$	0,0043	0,0057	0,0065	0,0086	0,0115	0,0144	0,0173	0,0202	–2,173	0,02899			
Kohlenmonoxid	CO	0,0193	0,0231	0,0249	0,0302	0,0366	0,0426	0,0481	0,0534	–0,783	0,10317	–0,067590	0,039450	–0,009470
Kohlendioxid	CO_2		0,0145	0,0165	0,0225	0,0306	0,0386	0,0463	0,0536	–3,882	0,05283	0,071460	–0,070310	0,018090
Kohlensuboxid	C_3O_2	0,0077	0,0110	0,0127	0,0183	0,0260	0,0335	0,0405	0,0472	1,362	–0,01657	0,267780	–0,322540	0,133290
Kohlenoxisulfid	COS	0,0095	0,0125	0,0140	0,0184	0,0242	0,0300	0,0356	0,0412	–4,089	0,06191	–0,004270		
Phosgen	CCl_2O		0,0076	0,0088	0,0125	0,0179	0,0238	0,0301	0,0368	–3,777	0,03554	0,021900		
Schwefelkohlenstoff	CS_2		0,0077	0,0087	0,0118	0,0159	0,0200	0,0241	0,0282	–3,468	0,04086	0,000210		
Schwefeldioxid	SO_2		0,0084	0,0095	0,0131	0,0183	0,0238	0,0292	0,0343	0,358	0,01312	0,069520	–0,032070	–0,008300
Schwefeltrioxid	SO_3				0,0172	0,0231	0,0287	0,0340	0,0391	–7,361	0,07104	–0,014220		
Sulfurylchlorid	Cl_2SO_2				0,0119	0,0159	0,0199	0,0238	0,0276	–3,541	0,04251	–0,002860		
Schwefelhexafluorid	SF_6		0,0118	0,0135	0,0184	0,0243	0,0296	0,0343	0,0384	–9,510	0,08657	–0,031860		

A.4 Graphical interfaces for user inputs

The graphical input interfaces for parameters and measurement data, as described in chapter 6.2.

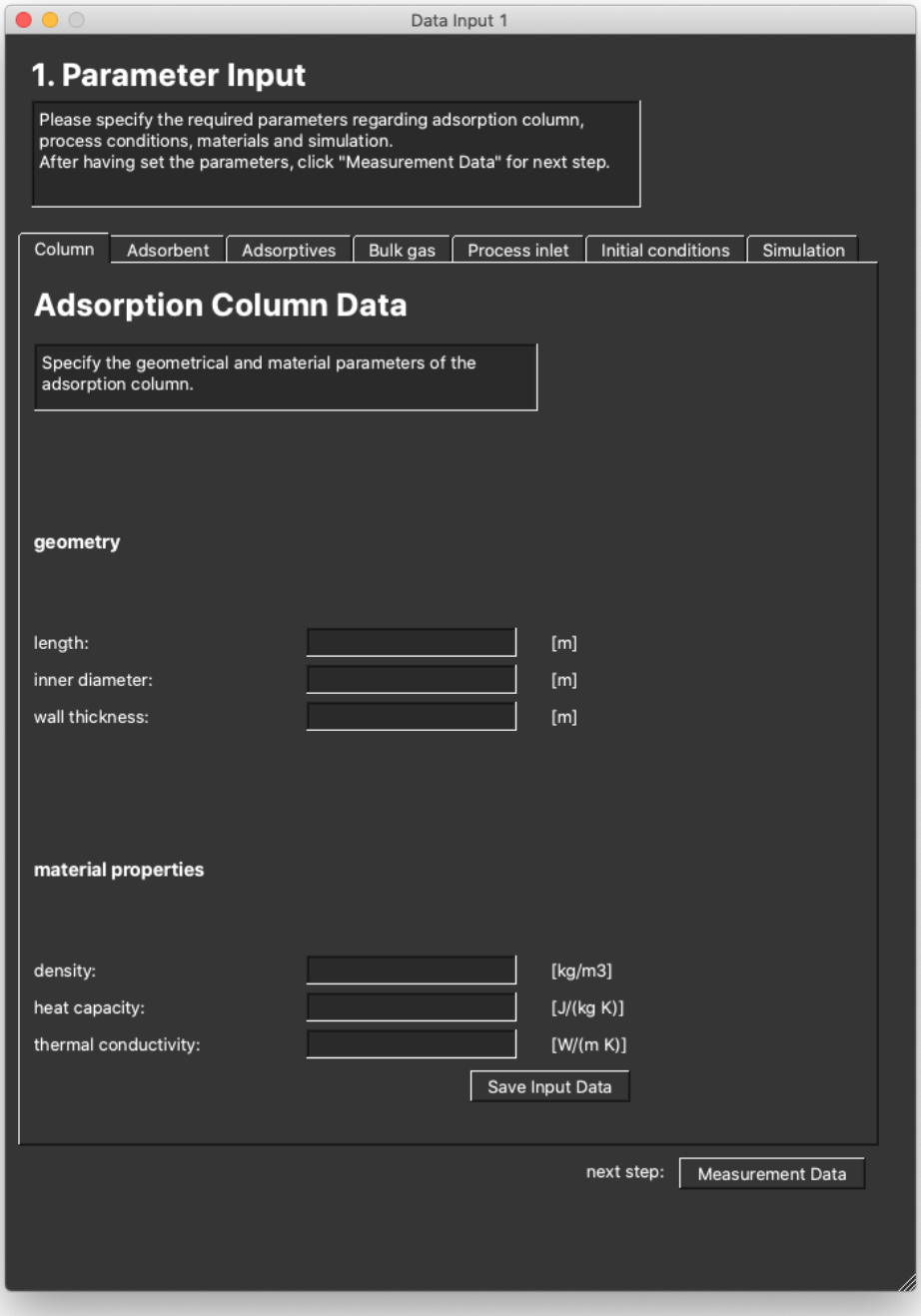

Figure A.2: Graphical user interface for entering and saving the required parameters

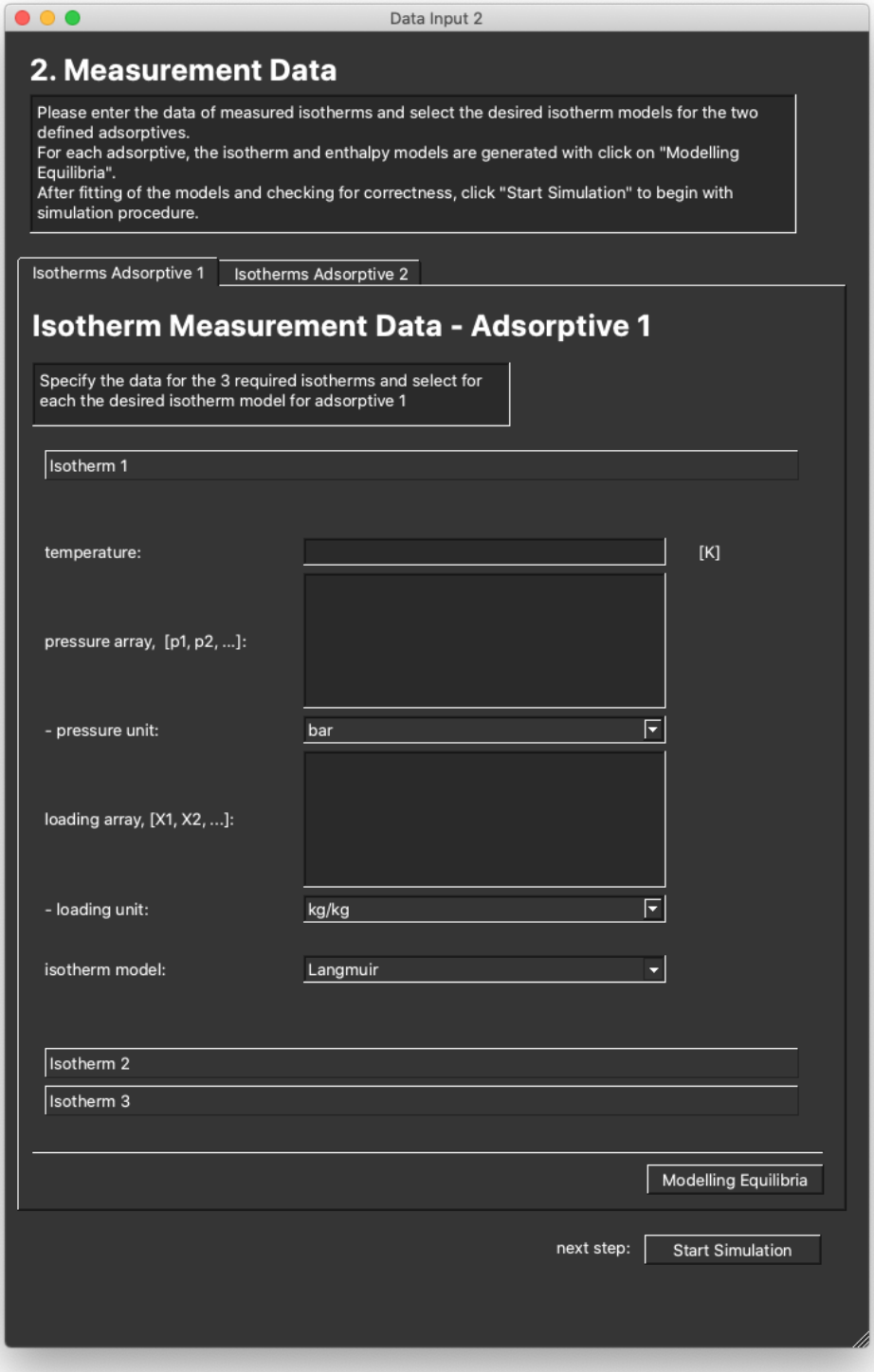

Figure A.3: Graphical user interface for entering and modelling equilibrium data

A.5 Graphical outputs for results analysis

The graphical output interfaces for mass transfer zones and heat curves, the rates of change for loadings, concentrations and temperatures, with user interaction on process timee as well as the breakthrough curves, as described in chapter 6.2.

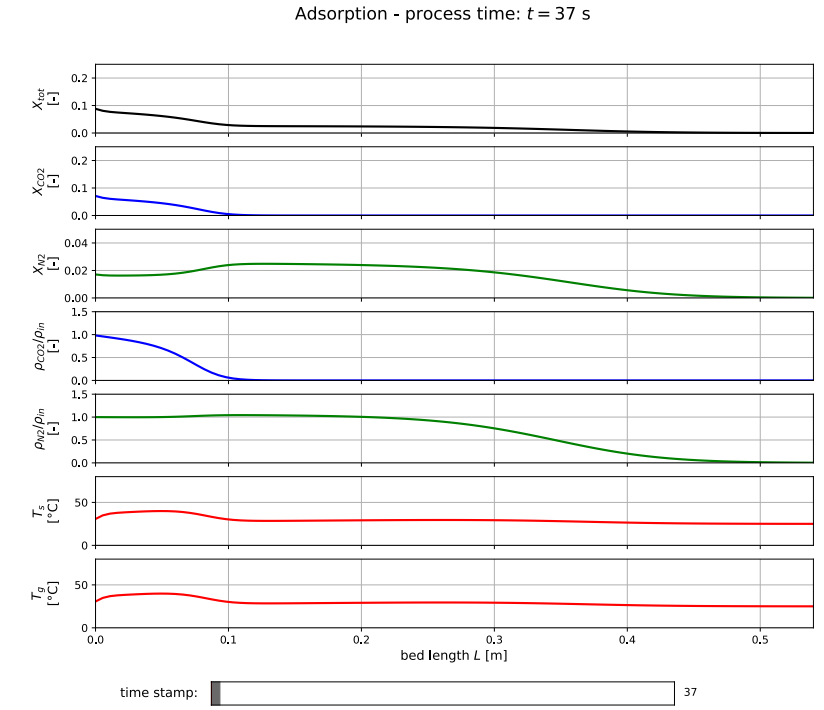

Figure A.4: Graphical output of mass transfer zones and heat curves, with user interaction on process time

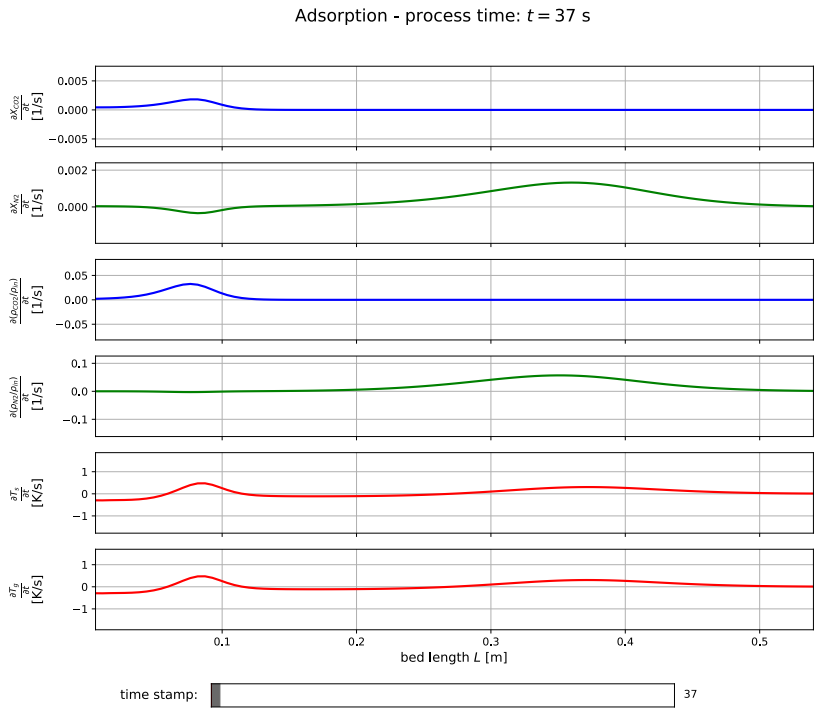

Figure A.5: Graphical output of of the rates of change for loadings, concentrations and temperatures, with user interaction on process time

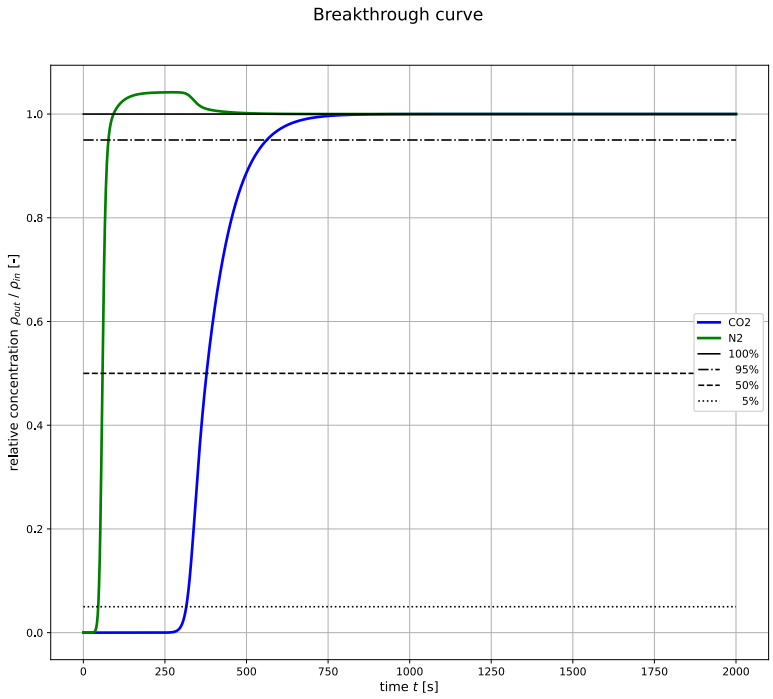

Figure A.6: Graphical output of the breakthrough curves with characteristic time values